ANALYSIS OF SELECTED THERMAL REACTOR BENCHMARK EXPERIMENTS BASED ON THE JEF-1 EVALUATED NUCLEAR DATA FILE

WOLFGANG BERNNAT
MARGARETE MATTES
MUHAMMAD ARSHAD
DIETER EMENDÖRFER
JÜRGEN KEINERT
BURKHARD POHL

MAY 1986

IKE 6-157
JEF REPORT 7

INSTITUT FÜR KERNENERGETIK UND ENERGIESYSTEME, STUTTGART
PROF. DR. RER. NAT. A. SCHATZ, PROF. DR.-ING. A. VOSS
ABTEILUNG REAKTORPHYSIK
PROF. DR. RER. NAT. D. EMENDÖRFER

ANSCHRIFT: IKE, PFAFFENWALDRING 31, 7000 STUTTGART 80

Abstract

For the validation of the evaluated nuclear data file JEF-1 in thermal reactor applications, especially beginning-of-life criticality calculations, a number of CSEWG thermal reactor benchmarks, 'high conversion' benchmarks, and critical experiment benchmarks for plutonium recycle in LWRs have been selected. These benchmarks cover light and heavy water moderated uranium metal, uranium oxide, and uranium-plutonium oxide lattices as well as homogeneous solutions of uranyl- and plutonium nitrate. In addition, for testing capture cross-sections of actinides, comparisons between calculated and experimental reaction rate ratios measured at the SHERWOOD assembly in the pool reactor MELUSINE (GRENOBLE-FRANCE) have been performed. Further, neutron thermalization benchmarks were chosen to validate JEF-1 scattering law data and thermal absorption cross-sections.

For the generation of multigroup cross-section libraries based on JEF-1 data the NJOY nuclear data processing system was used. The calculation of spectral weighted group-constants, critical parameters, and lattice cell reaction rate ratios have been performed using the IKE-RSYST/CGM program system. The effective multiplication factors (k_{eff}) of the different assemblies are calculated solving the 1D-neutron transport equation by means of the S_N-method (program ANISN).

Most of the JEF-1 results show an excellent agreement with corresponding experimental values (fast advantage and thermal disadvantage factors, cell reaction rate ratios, k_{eff}). For some assemblies, especially homogeneous plutonium solutions, the calculated values disagree with the experimental values by the same order as it is the case for ENDF/B-IV and V, respectively. For light water moderated uranium lattices, for which ENDF/B-IV data underestimate k_{eff} remarkably, JEF-1 results show a good agreement with experiments and are comparable with those from ENDF/B-V.

Contents

List of Figures

List of Figures (continued) Page

List of Tables

1 Introduction

The accurate determination of the reactivity of systems containing fissionable nuclides is important for both operating conditions of a power plant and criticality safety in the fuel cycle. The calculation of integral parameters such as multiplication factor, critical boron concentration, lattice cell reaction rates, advantage/disadvantage factors etc. is a complex procedure which requires appropriate basic nuclear cross-sections and adequate treatment of resonance absorption and thermal scattering. For validating calculation methods and nuclear data a large number of experimental values from "clean" and well documented critical experiments (benchmarks) and operating power plants are available.

To test the nuclear data contained in evaluated data files for thermal reactor applications it is important that the compositions and geometries of the considered benchmarks should be as simple as possible, so that difficulties of core representation do not undermine the comparison with experiment.

The main task of this work is to validate data from the Joint Evaluated File JEF-1 /1, 2/ for thermal reactors by calculating benchmark assemblies containing different fuels (U, Pu, mixed oxide) and moderators (H_2O, D_2O) and comparing with measured integral parameters such as k_{eff}, lattice cell reaction rate ratios and advantage/disadvantage factors. The Joint Evaluated File JEF-1 is the result of a scientific cooperation between laboratories in Austria, France, F.R. Germany, Italy, Japan, Netherlands, Sweden, Switzerland, United Kingdom and the NEA Data Bank.

Furthermore, it is desirable to have a comparison with results from other evaluated data files. Therefore, in addition results from benchmark calculations with ENDF/B-IV and ENDF/B-V /3/ are given too.

For the generation of pointwise and multigroup cross-section data based on evaluated data libraries in ENDF/B format the NJOY nuclear data processing system /4/ is an adequate tool which enables to calculate data for arbitrary energy structures, temperatures and weighting functions.

For most of the applications in the field of thermal reactors it is not necessary to start every problem from the evaluated data library using NJOY. From our experience multigroup libraries with about 100 groups for the fast and epithermal energy range, 8500 groups for the resolved resonance region and 151 groups for the thermal energy range are an adequate basis for epithermal and thermal

systems. From these libraries problem-dependent broad group cross-sections for the transport calculations can be generated by calculating a fine group cell spectrum for an idealized cell and using this spectrum as weighting function for collapsing to broad groups. For these spectral calculations the program system RSYST/CGM was used /5/. The solution of the transport equation for the simplified assemblies were performed with the 1D-S_N-program ANISN /6/.

For the validation of basic nuclear data and data processing systems the CSEWG thermal reactor benchmarks /7/ and 'high conversion' benchmarks /8/ cover a wide range of light water moderated homogeneous and heterogeneous systems with uranium or plutonium as fuel. These benchmarks have been analyzed with JEF-1 data and the results are discussed in this report.

2 Scope of Benchmarks

For the validation of the Joint Evaluated File JEF-1 data several neutron thermalization benchmarks and critical assemblies summarized in Table 2.1 were analysed. Most of these (experimental) benchmarks have been published in the CSEWG Benchmark Specification ENDF-202 /7/. The nuclides appearing in these benchmark calculations are listed in Table 2.2.

2.1 Neutron Thermalization Benchmarks

To validate the (JEF-1/NJOY) multigroup neutron cross-sections and scattering matrices for the thermal energy range comparisons of calculated and measured neutron spectra have been performed. Corresponding experiments are described in /9 - 11/. They are essentially infinite medium neutron spectra measurements in homogeneous mixtures of moderators (H_2O, D_2O) and absorbers at different temperatures. They provide useful checks for neutron scattering law data.

2.2 Thermal Reactor Benchmarks

2.2.1 U-235-H_2O Systems

- ORNL-1, 2, 3, 4, 10

  Five unreflected spheres of U-235 (as uranyl nitrate) in H_2O are considered, three of them poisoned with boron. Critical compositions and volumes are specified. These assemblies are primarily sensitive to H_2O scattering data, the thermal capture cross-sections of U-235 and hydrogen, the U-235 thermal fission cross-section and the average number of neutrons per fission /7/.

2.2.2 Low Enriched Uranium-H_2O Systems

- TRX-1, 2, 3, 4

  These are H_2O-moderated, fully reflected simple assemblies operated at room temperature. The fuel rods consist of uranium metal (enriched to 1.3 % U-235)

Table 2.1: Selected thermal reactor benchmarks and experiments for validation of JEF-1 data

Assembly	Moderation ratio	Comments
	N_H/N_{U-235}	
ORNL- 1	1378	Ref. /7/; highly enriched (94 wt%) homo-
- 2	1177	geneous uranyl nitrate solutions (unre-
- 3	1033	flected spheres, partly poisoned with
- 4	972	B-10).
-10	1835	Measured parameters: k_{eff}.
	V_{mod}/V_{fuel}	
TRX-1	2.35	Ref. /7/; 1.3 wt% U-235 enriched latti-
-2	4.02	ces with metallic fuel (fully reflected).
-3	1.00	Fuel rod diameter 0.983 cm, aluminium
-4	8.11	clad.
		Measured parameters: advantage + disadvan-
		tage factors, cell reaction rate ratios,
		k_{eff}.
BAPL-UO_2-1	1.43	Ref. /7/; 1.31 wt% U-235 enriched lattices
-2	1.78	with oxide fuel (fully reflected). Fuel
-3	2.40	rod diameter 0.9728 cm, aluminium clad.
		Measured parameters: disadvantage factors,
		cell reaction rate ratios, k_{eff}.
HIC-UO_2- 3	1.37	Ref. /8/; 3.04 wt% enriched UO_2 pellets of
-10	0.96	0.935 cm diameter in aluminium tubes with
-11	0.76	various water-to-fuel volume ratios (fully
-13	0.43	reflected)
		Measured parameters: k_{eff}.
SHERWOOD (Grenoble)		Ref. /12/; actinides capture cross- sections measurements in PWR spectrum.

Assembly	Moderation ratio	Comments
	N_H/N_{Pu}	
PNL- 1	668	Ref. /7/; critical spheres of plutonium
- 2	125	nitrate solutions (PNL-7 and PNL-12 water
- 3	1154	reflected), up to 4.6 atom % Pu-240.
- 4	873	Measured parameters: k_{eff}.
- 5	554	
- 6	125	
- 7	980	
- 8	758	
-12	1067	
- Inf. Med.	3695	Infinite critical solution of Pu-239 in H_2O
	V_{mod}/V_{fuel}	
PNL-30	1.194	Ref. /7, 13, 14/; clean critical experi-
-31	1.194 *)	ment benchmarks for plutonium recycle in
-32	2.524	LWR's. Six lattices with UO_2-2 wt% PUO_2
-33	2.524 *)	(8 % Pu-240), Zircaloy-2 clad.
-34	3.640	*) boron poisoned
-35	3.640 *)	Measured parameters: k_{eff}.
	V_{mod}/V_{fuel}	
MIT-1	20.765	Ref. /7, 3/; D_2O-moderated lattices of
-2	25.897	natural uranium rods with diameters of
-3	34.608	2.565 cm in a triangular lattice pattern.
		Measured parameters: cell reaction rate
		ratios, k_{eff}.

Table 2.2: Nuclides used in benchmark calculations for validation of JEF-1

Isotope	MAT	Type of Benchmark							
		Thermal	U-nitrate ORNL	Pu-nitrate PNL	UO_2-lattices BAPL-UO_2 HI-C	U-metal lattices TRX	MOX lattices PNL	D_2O-lattices MIT	SHERWOOD-experiment
H	4011	+	+	+	+	+	+	+	+
	4001	+	+	+	+	+	+	+	+
D	4012	+						+	
	4002	+						+	
B-10	4050	+	+				+		
N-14	4074	+	+	+					
O-16	4086	+	+	+	+	+	+	+	+
Al-27	4137				+	+		+	
Fe	4260			+					
Zr	4409						+		+
Dy-164	4664					+			
Lu-176	4716					+			
U-234	4924		+						
U-235	4925		+		+	+	+	+	+
U-236	4926		+						
U-238	4928		+		+	+	+	+	+
Pu-238	4948	+							
Pu-239	4949	+		+			+		+
Pu-240	4940	+		+			+		+
Pu-241	4941	+		+			+		+
Pu-242	4942	+		+			+		+
Am-241	4951	+							+
Am-243	4954								+

cladded in aluminium. They are 48 inches long and 0.387 inch in diameter and are arranged in triangular lattices. TRX-1 and TRX-2 are uniform lattices with moderator/fuel volume ratios of 2.35 and 4.02, respectively. TRX-3 and TRX-4 are two-region assemblies in which the test lattice is surrounded by a driver of UO_2 rods. The moderator/fuel volume ratios are 1.00 and 8.11 respectively.

The following integral parameters are measured at the center of each lattice: the epithermal/thermal ratio of U-238 capture (ρ^{28}) and U-235 fission (δ^{25}), the ratio of U-238 capture to U-235 fission (C*), and the ratio of U-238 fission to U-235 fission (δ^{28}). Also measured are axial bucklings for all lattices and radial bucklings for the uniform lattices.

The experiments at the TRX assemblies allow to test the U-235 resonance fission integral and thermal fission cross-section. They also test U-238 shielded resonance capture and the thermal capture cross-section, the U-238 fast fission cross-section, U-238 inelastic scattering, and the U-235 fission spectrum.

- BAPL-UO_2-1, 2, 3

These are H_2O-moderated, fully reflected simple assemblies operated at room temperature. The fuel rods are of high-density UO_2 (1,3 % U-235) cladded in aluminium. They are 48 inches long and 0.383 inch in diameter, arranged in triangular lattices with moderator/fuel volume ratios of 1.43, 1.78 and 2.40 respectively.

Integral parameter and B^2 measurements similar to those for the TRX assemblies are available. The cross-section sensitivities are comparable to the TRX experiments, but they are more representative to LWR-fuel.

- HI-C UO_2-3, 10, 11, 13

The HI-C-assemblies /8/ allow the study of reactor systems having tight lattices. Reactors with high conversion ratios become increasingly important in the utilization of nuclear energy. The high-conversion experiments extended the range of H-to-U-238 atom ratios from 5 to as low as 0.5. This corresponds

to water-to-fuel volume ratios ranging from 1.7 to 0.16. For the test of JEF-1 data four cores with Al-cladding and H-to-U-238 atom ratios from 4.15 to 1.32 have been selected.

- SHERWOOD assembly

The SHERWOOD assembly /12/ consists of a 5 x 5 square lattice of typical PWR fuel rods (from a 17x17 assembly). This system was irradiated in the pool reactor MELUSINE (Grenoble, France). The SHERWOOD experiment is useful for the validation of actinides capture cross-sections in a PWR neutron spectrum at operating temperatures.

2.2.3 Pu-H_2O Systems

- PNL-1 through 8 and 12

These are nine homogeneous aqueous plutonium nitrate assemblies with hydrogen/Pu-239 ratios ranging from 131 to 1204. The last three assemblies are reflected ones. Experimental values for critical volumes and compositions are available. In addition, an infinite homogeneous critical solution of Pu-239 in water is considered. The PNL-assemblies are generally useful for testing H_2O scattering data, cross-sections for resonance and thermal fission of Pu-239 and the Pu-239 fission spectrum.

2.2.4 UO_2-PuO_2-H_2O Systems

- PNL-30 through 35

These H_2O moderated mixed oxide lattices are fueled by compacted particles of UO_2-2wt% PuO_2 with 8 % Pu-240. The fuel rods are zircalloy cladded and arranged in a square lattice. Critical configurations are specified for three lattice spacings with borated and unborated moderator.

The lattices are useful for testing the U-235 and Pu-239 neutron cross-sections and fission spectra as well as the cross-sections of U-238, Pu-240 and water.

2.2.5 U-235-U-238-D_2O Systems

- MIT-1 through 3

The MIT-1, 2 and 3 benchmarks consist of D_2O-moderated lattices of natural uranium rods with diameters of 2.565 cm arranged in a triangular lattice pattern. The associated lattice spacings are 11.43, 12.70 and 14.605 cm. Measured lattice parameters include B^2, ρ^{28}, δ^{25}, δ^{28}, and C*.

These lattices are useful for testing D_2O cross-section data and cross-sections for thermal and epithermal U-235 fission, thermal and epithermal U-238 neutron capture, and U-238 fast fission.

3 Method of Calculations

The calculation of parameters measured in the benchmark-experiments is divided into three parts:

- Generation of multigroup cross-section libraries for the fast, resonance and thermal energy range for the nuclides given in Table 2.2.
- Spectral calculations for generation of weighted broad group cross-sections.
- Transport calculations for determination of k_{eff}, reaction rate ratios etc.

For the generation of multigroup cross-section libraries the NJOY nuclear data processing system /4/ was used. These libraries are the data base for the spectral code RSYST/CGM described in section 3.2.

The selected benchmarks can be calculated with sufficient accuracy by means of the 1D-S_N- method using broad group cross-sections from CGM. The main details of the transport calculations are described in section 3.3.

3.1 Generation of Problem-Independent Multigroup Cross-Sections

The CGM library consists of three separate sections:

- the 'thermal' library for the energy range from 10^{-5} to 3.059 eV with 151 groups,
- the 'fast' library for the fast and epithermal energy range from 0.414 eV to 14.98 MeV with 100 groups in GAM-II structure,
- the 'resonance' library for the resonance region from 0.876 eV to 4.3 keV with 8500 groups.

They differ in contents and format although the basic data source and processing methods were identical.
The cutoff-energy between thermal and epithermal/fast energy range can be chosen before running the spectral module CGM.

Many of the NJOY processing methods /4/ used to prepare the CGM libraries apply to all cross-section processing problems. The following discussion will concentrate on those particular methods of most interest for thermal reactor problems. The processing path through the modules of NJOY is shown in Fig. 3.1.

The RECONR module reconstructs resonance representations and interpolation laws given in ENDF-5 format so as to obtain a pointwise JEF-1 tape (PENDF) where all cross-sections are represented within specified tolerances by tables with linear interpolation. The PENDF tape is written in a format similar to the original ENDF format. In the BROADR module, the cross-sections are Doppler broadened and thinned. The UNRESR module is used when self-shielded average cross-sections for the unresolved energy region are required, and the THERMR module is used to compute energy-to-energy thermal scattering kernels and the thermal elastic scattering cross- sections (if any). The latter two NJOY modules add their results to the PENDF tape using non-standard formats in ENDF File 2 and File 6, respectively. The final product of this process is a PENDF tape containing pointwise versions of the cross-sections required for the thermal reactor libraries. The tolerance used for reconstructing the resonance cross sections and for Doppler-broadening was 0.1 percent.

The GROUPR module is used to obtain multigroup averages. Because each of the three libraries has different group structure and weighting requirements, three separate passes through GROUPR are required. However, only a single PENDF tape had to be prepared.
For the smooth component of the weighting function in the narrow resonance approximation (NR) the following form was used:

$$W(E) = \text{'Thermal'} + 1/E + \text{'Fission'}$$

where 'Thermal' and 'Fission' stand for Maxwellian spectrum and for fission spectrum, respectively.

The final step is to transform the multigroup cross-sections into the RSYST/CGM format.

- Thermal Library

The CGM thermal library contains fission and absorption cross-sections, P_L scattering matrices (i.e., group-to-group cross-sections) and fission yield ($\bar{\nu}$). A transport cross-section is included for later use in calculating diffusion coefficients.

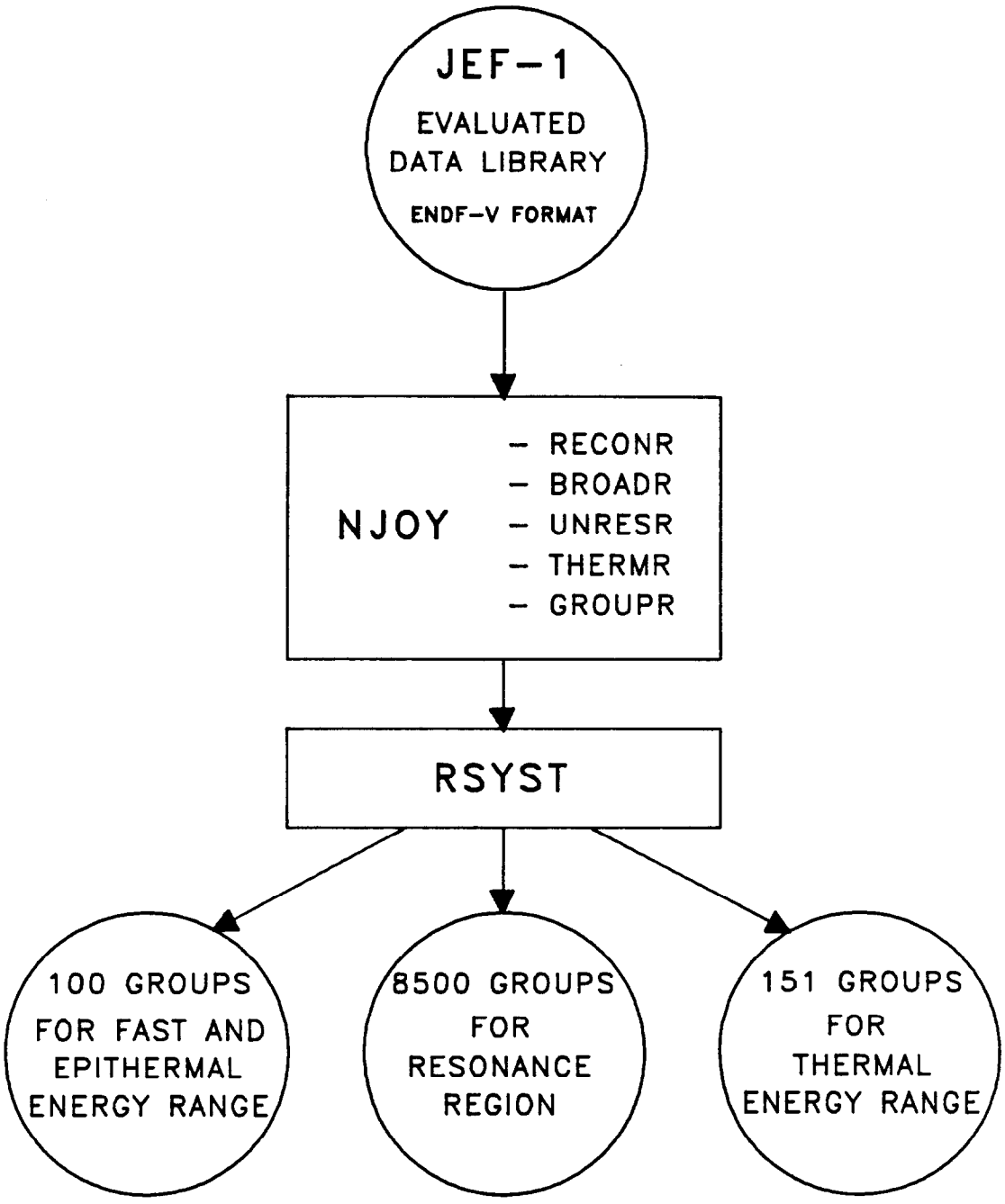

Fig. 3.1: Generation of multigroup cross-section libraries for calculation of thermal fission systems

The scattering matrices for all nuclides but 'H(H_2O)' (that is, hydrogen bound in water) and 'D(D_2O)' were computed with the free gas model. The above two were computed using scattering law data from JEF-1. The total cross-section and the P_1 matrix were used to compute a detailed transport cross-section for the library to take into account an energy-dependent $\bar{\mu}$.

Cross-sections and matrices were computed using the group structure of Table A.1 given in Appendix. The weighting function used was a hardened Maxwellian spectrum below 100 meV.

- Fast Library

The fast (or 'epithermal') calculation in CGM requires fission and/or absorption cross-sections, fission spectra and fission yield ($\bar{\nu}$), P_L scattering matrices (composed of up to P_3 elastic, inelastic, n,2n etc.) and shielded cross sections for fission and/or absorption, and scattering are given for several values of temperature and 'background cross-section' σ_o.

The group structure used for this library is the GAM-II structure given in Table A.2 in the Appendix. The smooth component of the weighting function is assumed to be composed of 1/E and a fission spectrum with the cut-off energy at 0.82 MeV.

The fast library includes steady-state fission spectra for all fissionable isotopes.

- Resonance Library

This library contains temperature dependent ultrafine group cross-sections for fission and/or absorption, and elastic scattering in the resonance region, mainly for U and Pu isotopes. In addition, for the main resonance absorber U-238 group data for different σ_o -values have been calculated. This allows a detailed spectrum calculation taking into account interference and self-shielding effects. For more details see section 3.2.

The 8500 energy groups are equidistant in lethargy with $\Delta u = 0.001$ and span the energy range from 0.876 eV up to 4.307 keV (corresponding to the GAM-II energy group structure).

3.2 Generating of Problem-dependent Broad Group Data

For the transport calculations, carried out mainly by the 1D S_N-method, the number of energy groups must be reduced from 100/8500/151 to 30-60 groups for the whole energy range. All weighting spectra for collapsing multigroup data were calculated by means of the RSYST/CGM program. A flow chart of the main parts of CGM is shown in Fig. 3.2. RSYST is a general module system for computer aided calculations and CGM is the cross-section generation (spectral calculation and broad-group collapsing) module of RSYST. CGM is based on a combination of the first collision probability method and the B_N-theory. In addition, in the fast and resonance energy range the NR-approximation is used as weighting function for the multigroup (100 and 8500) libraries.

As an example, the representation of the absorption cross-section of the important nuclide U-238 in the fast and epithermal energy range is shown in Fig. 3.3 (below 4 keV only the data of the 8500 group library are drawn). A comparison of these multigroup cross-sections (U-238 absorption) for two different NR-weighting functions (50 barn and infinite as background cross-section σ_0, respectively) is shown in Fig. 3.4. Differences of more than 30 % were found in the fine group cross-sections (even in the hyper-fine 8500 group library).

By an interpolation in respect to the correct background cross-section of every group, especially for the main resonance absorber U-238, this effect will be taken into account by CGM. The effect becomes important, if the spectrum will be hardened (e.g. in the case of tight lattices as for the high conversion-"HIC"-experiments).

In CGM the first collision theory is used for the isotropic one-dimensional spectral calculation. A variable number of mesh intervals in fast, resonance, and thermal energy ranges allows to achieve desired optimum accuracies in each energy range according to the nature of the problem. In the resolved resonance region the one-dimensional calculations are carried out for an ultrafine group structure (8500 groups). In addition to the treatment of a general cell (with any number of mesh intervals) a very efficient 2-region option is also available for the resonance calculations.

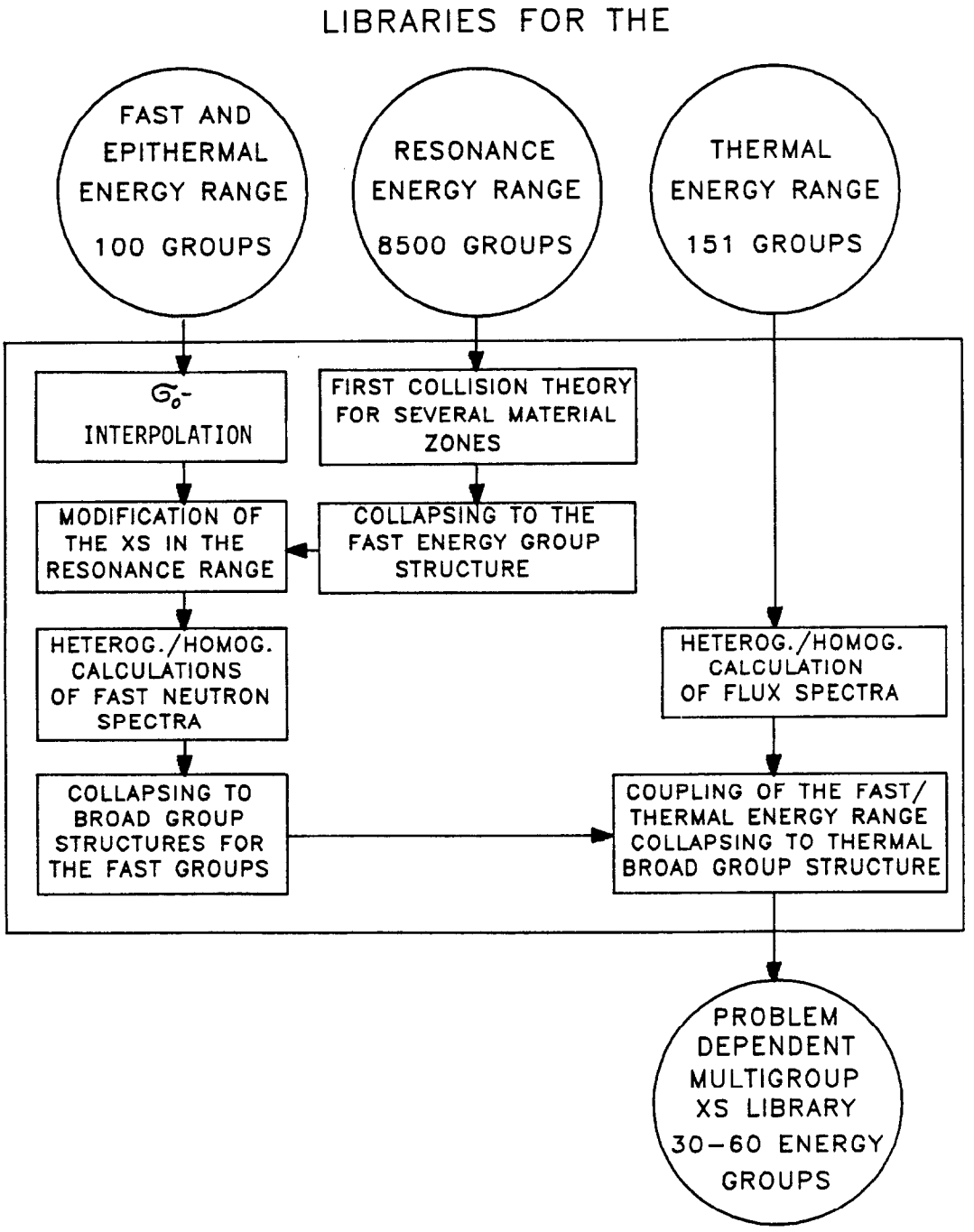

Fig. 3.2: The RSYST/CGM module for cross-section processing for thermal reactor calculations

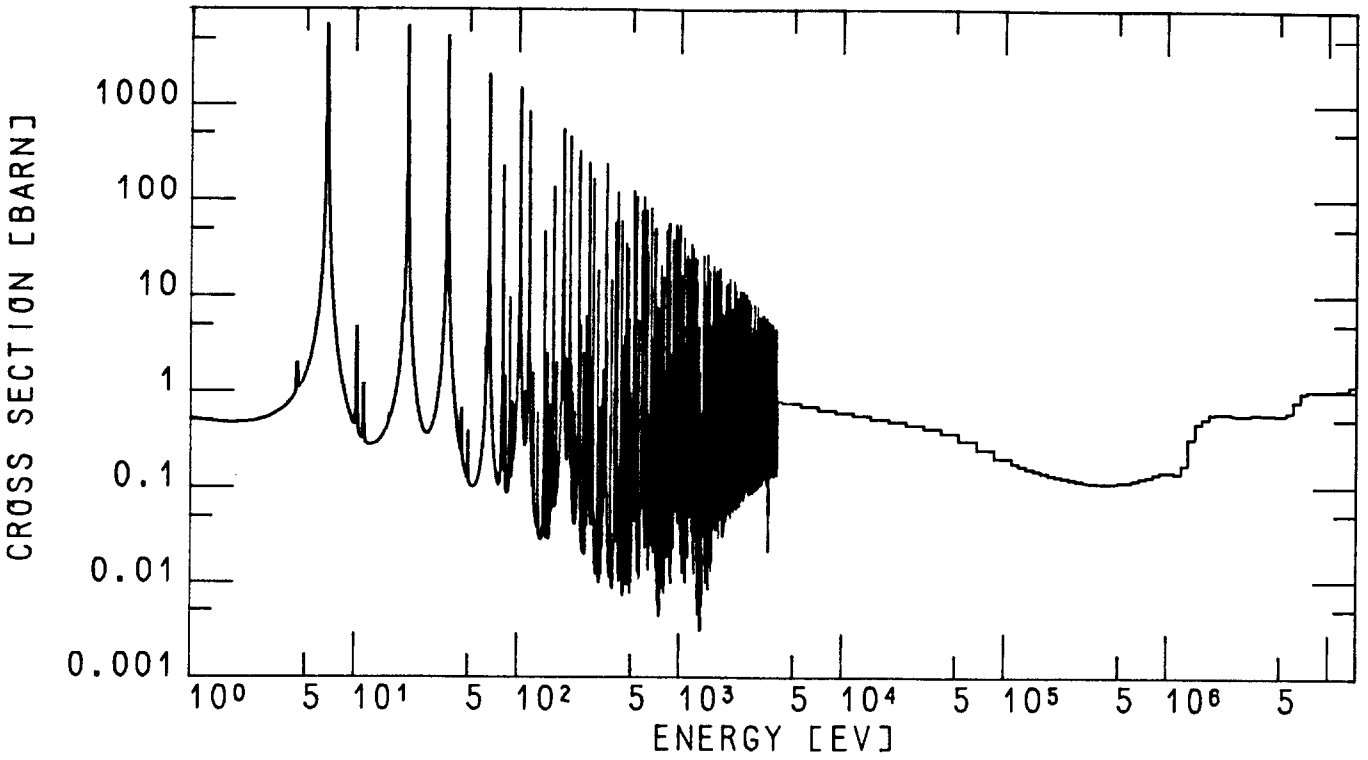

Fig. 3.3: U-238 absorption cross-section in 8500 energy group structure (E < 4 keV) and 100 group structure (E > 4 keV)

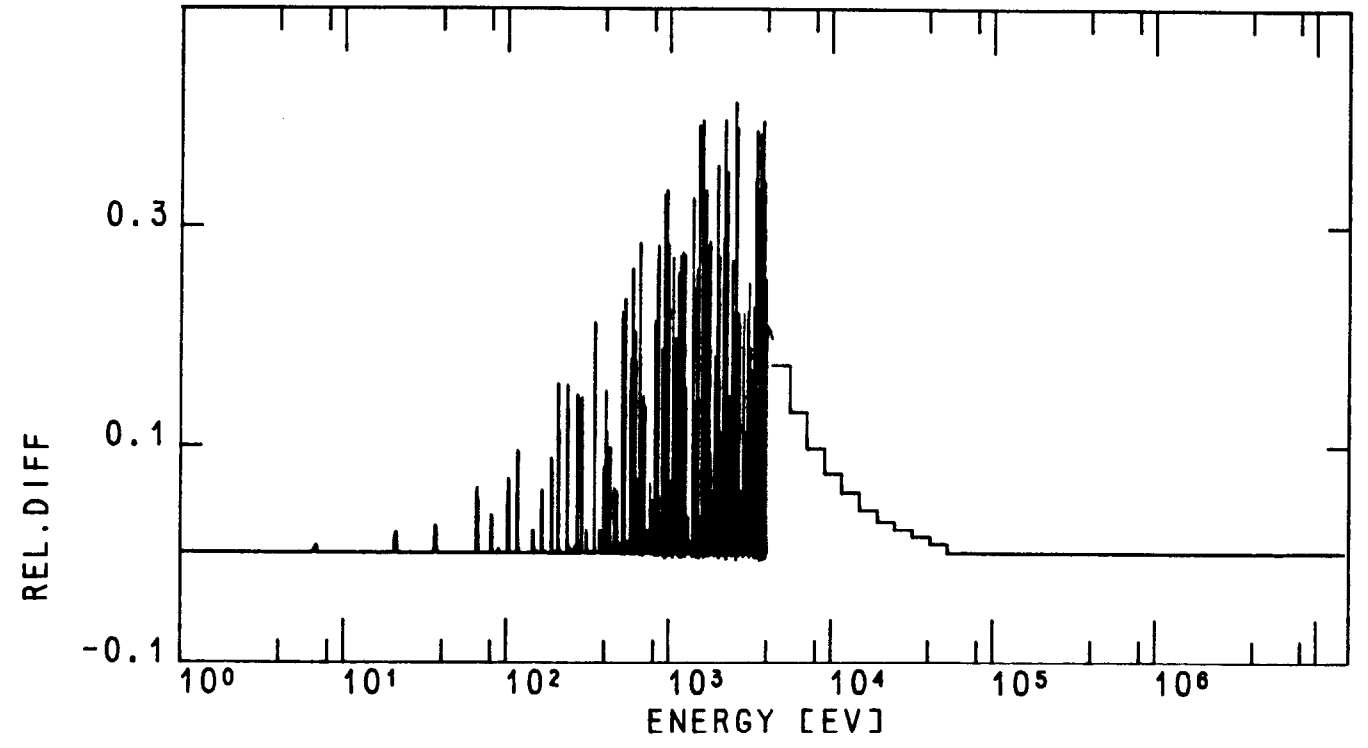

Fig. 3.4: Relative difference $(\sigma_a(\sigma_o = \infty) - \sigma_a(\sigma_o = 50\ b))/\sigma_a(\sigma_o = \infty)$ of the U-238 absorption cross-section in the 100 and 8500 group library

As mentioned above in the unresolved (and also resolved) resonance region a weighting function based on the NR-approximation is used for the generation of multigroup cross-sections (100 group and 8500 group libraries). The weighting function is defined by following expression:

$$\phi(E) = \frac{S(E)}{N_o(\sigma_t+\sigma_o)} \quad ,$$

where S(E) is a weak energy dependent function (e.g. fission spectrum in fast and 1/E in slowing down energy range),

N_o	the nuclide density of the resonance absorber for which the spectrum is calculated,
$\sigma_t(E)$	total cross section of resonance absorber,
$\sigma_o = \frac{1}{N_o}(\sum_{i\neq 0} \sigma_t^i N_i + \sigma_e)$	background cross-section,
$\sigma_e = \frac{1-c}{\bar{l}}$	escape cross-section for heterogeneous case,
c	Dancoff-factor,
$\bar{l}$	mean chord length of the lattice.

Cross sections of the resonance nuclides are tabulated for a number of values of the background cross sections (σ_o). The energy dependent background cross sections for each nuclide are then evaluated according to the problem. The effects of the cell heterogeneity and interaction between absorber lumps are also taken into account by adding the escape cross section to the σ_o value for each nuclide. The cross sections are then interpolated for each nuclide according to its background σ_o.

For the analysis of the benchmark problems mentioned in this report, the cut-off energy between the resonance and thermal regions was taken to be 3.059 eV. No upscattering was considered above this energy. The temperature dependence of the cross sections above cut-off energy was taken into account, however. The resonances of certain isotopes lying below the cut-off energy were supposed to be covered adequately by the relative small width of thermal groups in this region.

After the one-dimensional spectral calculations the cross sections for the cell are homogenized and B_n calculations are performed for the homogeneous cell to take into account the leakage. Then the cross sections of the individual nuclides as well as for the cell can be collapsed to any desired broad group structure. The zonal and cell reaction rates are evaluated too. The broad group cross sections are then used for the one-dimensional transport calculation. For illustration of the resonance treatment in CGM the neutron flux spectra in fuel and moderator of a typical PWR-lattice calculated for the 8500 group library are shown in Figs. 3.5 and 3.6, respectively. Using these spectra, a high degree of accuracy for the calculated resonance integral of U-238 can be achieved.

As an example, the broad group microscopic absorption cross-section is plotted in Fig. 3.7 for both the TRX-1 and BAPL-UO_2-3 lattice. The water/fuel volume ratios of these lattices are identical, however the TRX-fuel has a much higher uranium density (metallic fuel) than the BAPL-UO_2 fuel, with the consequence of smaller broad group cross sections (here 60 groups) in the resolved resonance region of U-238.

After these explanations one can summarize the main features of CGM:

- CGM uses three multigroup libraries for fast, resonance and thermal range.
- The group numbers and structures of these libraries are not fixed.
- The cross sections in the libraries are given for several temperatures and - in the fast and resonance range - different σ_o-values.
- CGM interpolates for actual temperatures and σ_o-values (for important resonance absorbers).
- CGM performs spectral calculations for all energy ranges by means of a first collision method for 1D-lattice geometry, using an arbitrary number of meshes for fuel, cladding and moderator (for heterogeneous cases).
- There is a fast 2-region option for the treatment of resonance energy range.
- The leakage is taken into account by performing B_N calculations (N = 0-3) using appropriate bucklings and homogenized cross-sections (from the 1D-calculations).
- CGM generates broad group cross sections for transport- and diffusion calculations.
- CGM calculates $k_{infinity}$ and reaction rates for the broad groups as well as for one and two groups.

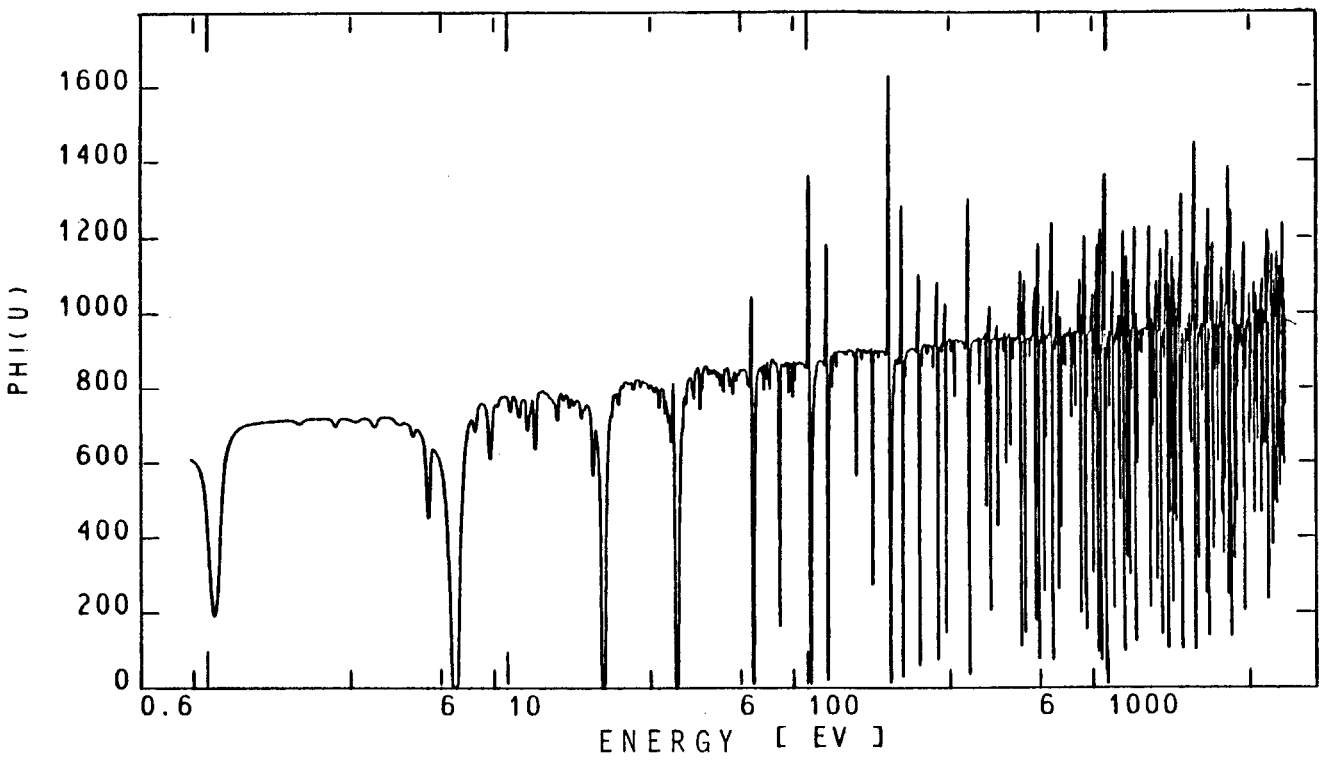

Fig. 3.5: Neutron flux spectrum in the fuel rods of a typical PWR lattice

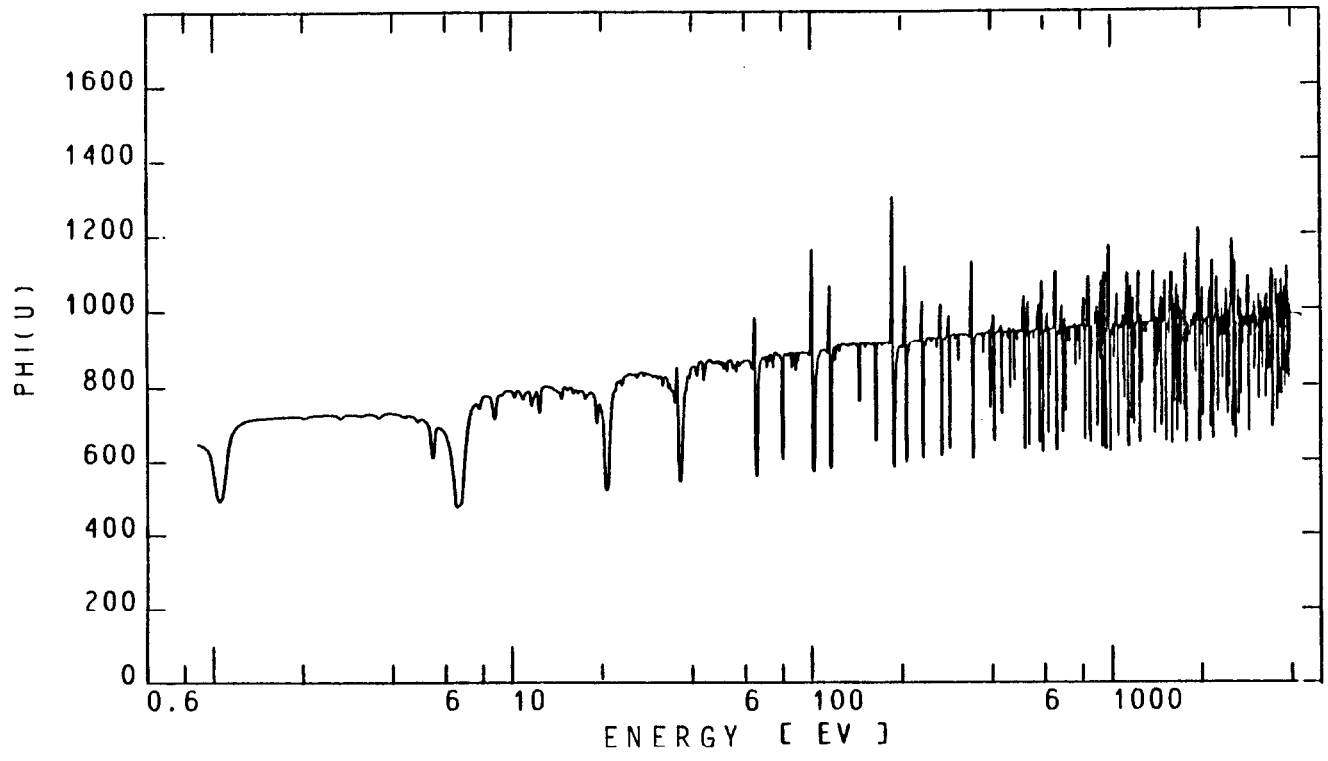

Fig. 3.6: Neutron flux spectrum in the moderator zone of a typical PWR lattice

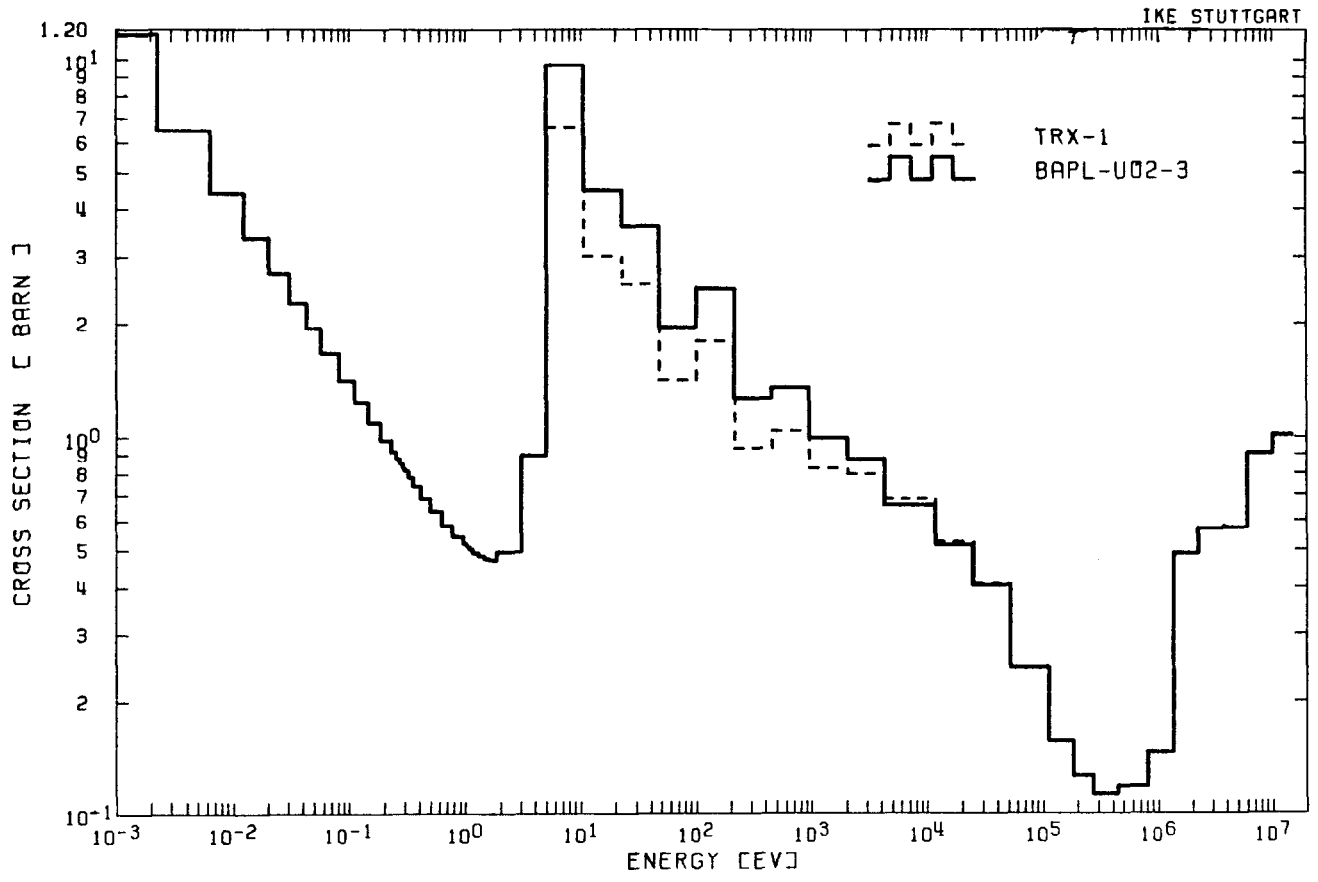

Fig. 3.7: σ-absorption for the uranium benchmark lattices TRX-1 and BAPL-UO_2-3 ($V(H_2O)/V(Fuel) = 2.4$) at room temperature

3.3 Transport Calculations

The criticality calculations for the different benchmark assemblies have been performed using the 1-D S_N-transport code ANISN /6/. In the transverse direction the experimental bucklings were used to take into account the axial leakage (for cases with cylindrical geometry).

The basic libraries were collapsed by means of CGM to 60 broad groups covering the energy range from 0.00001 eV to 15 MeV. For some assemblies the number of broad groups was lower (e.g., 30 groups for HI-C).

The transport calculations were mainly performed in S_4/P_1 approximation. This is an adequate assumption because in a former study /15/ we found nearly the same results for S_4/P_1- and S_{16}/P_3-calculations. For the D_2O and ORNL-benchmarks S_8/P_3-calculations were used to achieve sufficient agreement to experimental k_{eff}. The weakly absorbing D_2O systems are thought to be sensitive with respect to energy dependent bucklings, as it is the case for the neutron thermalization benchmarks.

Generally, the calculated k_{eff} are sensitive to the used fission spectra. For uranium or plutonium systems the deviation may be about $\Delta k = 0.002$. Therefore, for all benchmarks with several fissionable nuclides fission rate weighted fission spectra were generated.

4 Results for the Selected Benchmarks

For all in Table 2.1 listed thermal reactor benchmarks as well as for different neutron thermalization benchmarks results of JEF-1 - RSYST/CGM calculations will be presented in this chapter. The JEF-1 results will be compared with experimental values and - if available - with corresponding values calculated from other institutions using ENDF/B-IV and -V.

4.1 Neutron Thermalization Benchmarks

For the test of the thermal scattering law data thermal neutron spectra for different compositions and temperatures have been calculated solving the B_1-equations for 151 groups below 3.059 eV based on the JEF-1 scattering law data /16/. The calculated spectra are presented in Figs. 4.1 through 4.5.
Fig. 4.1 shows the neutron spectrum in pure light water at room temperature. This benchmark provides the most sensitive test of the JEF-1 scattering law data since no additional absorber will harden the spectrum. Fig. 4.2 shows the infinite medium neutron spectrum for a plutonium nitrate solution with 197.9 g Pu/l. Figs. 4.3 and 4.4 show infinite medium neutron spectra in borated water at room temperature and 316 C respectively. The analysed borated systems and the Pu-system validate the combination of both absorber data and scattering law data for the important temperature range of light water.

Comparing experimental results and theory, the overall agreement for H_2O-moderator is very satisfactory. Generally, the calculated spectra are within the quoted accuracy of measurement in the important energy range.

Fig. 4.5 shows the neutron spectrum in borated D_2O at room temperature. The agreement of theory and measurement is as excellent as it is for light water. However, the more important test for non-borated D_2O could not be carried out due to lack of experimental data.

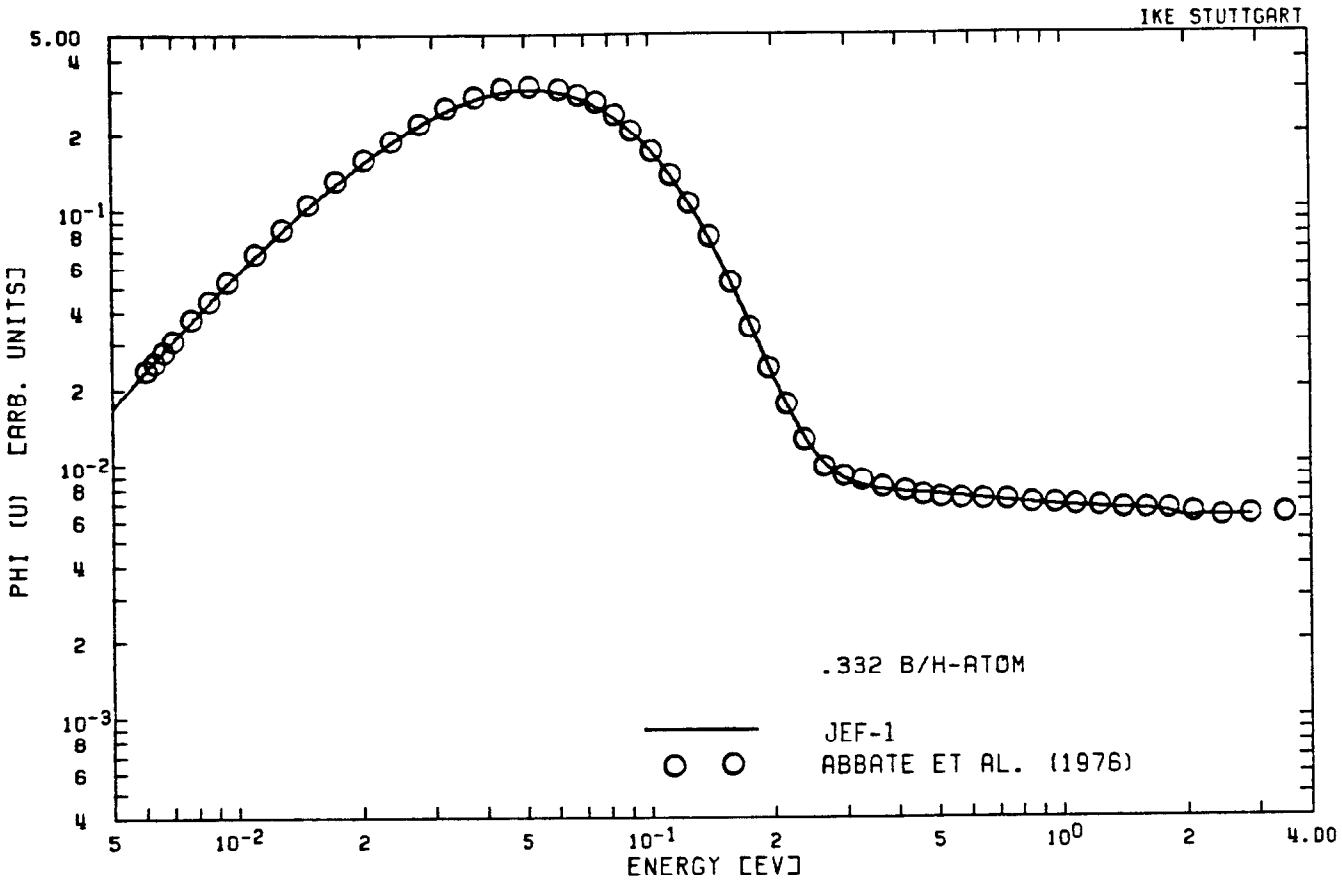

Fig. 4.1: Infinite medium neutron spectrum in pure water (H_2O) at T = 23 C

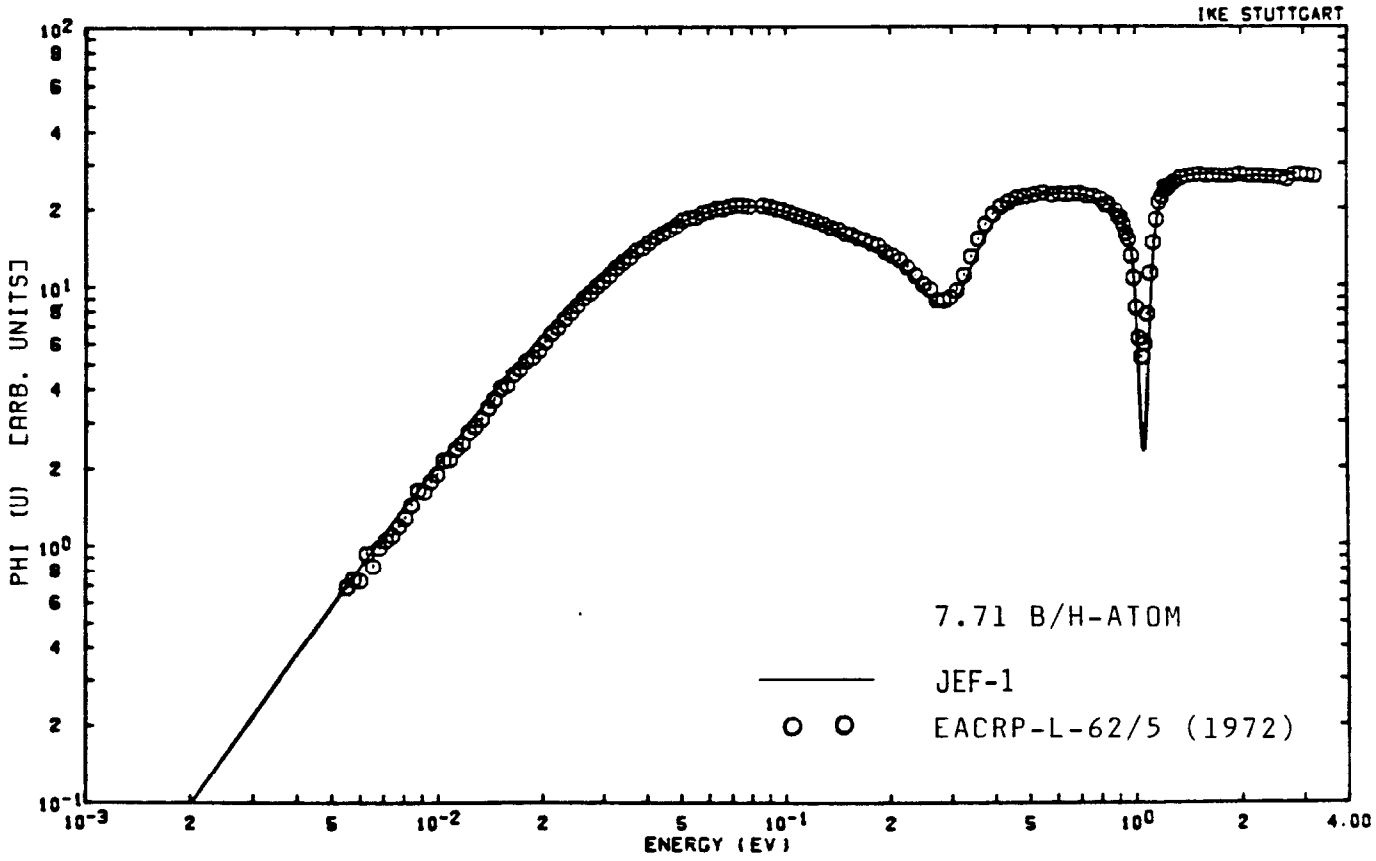

Fig. 4.2: Infinite medium neutron spectrum in a plutonium nitrate solution (197.9 g Pu/l at 23 wt% Pu-240)

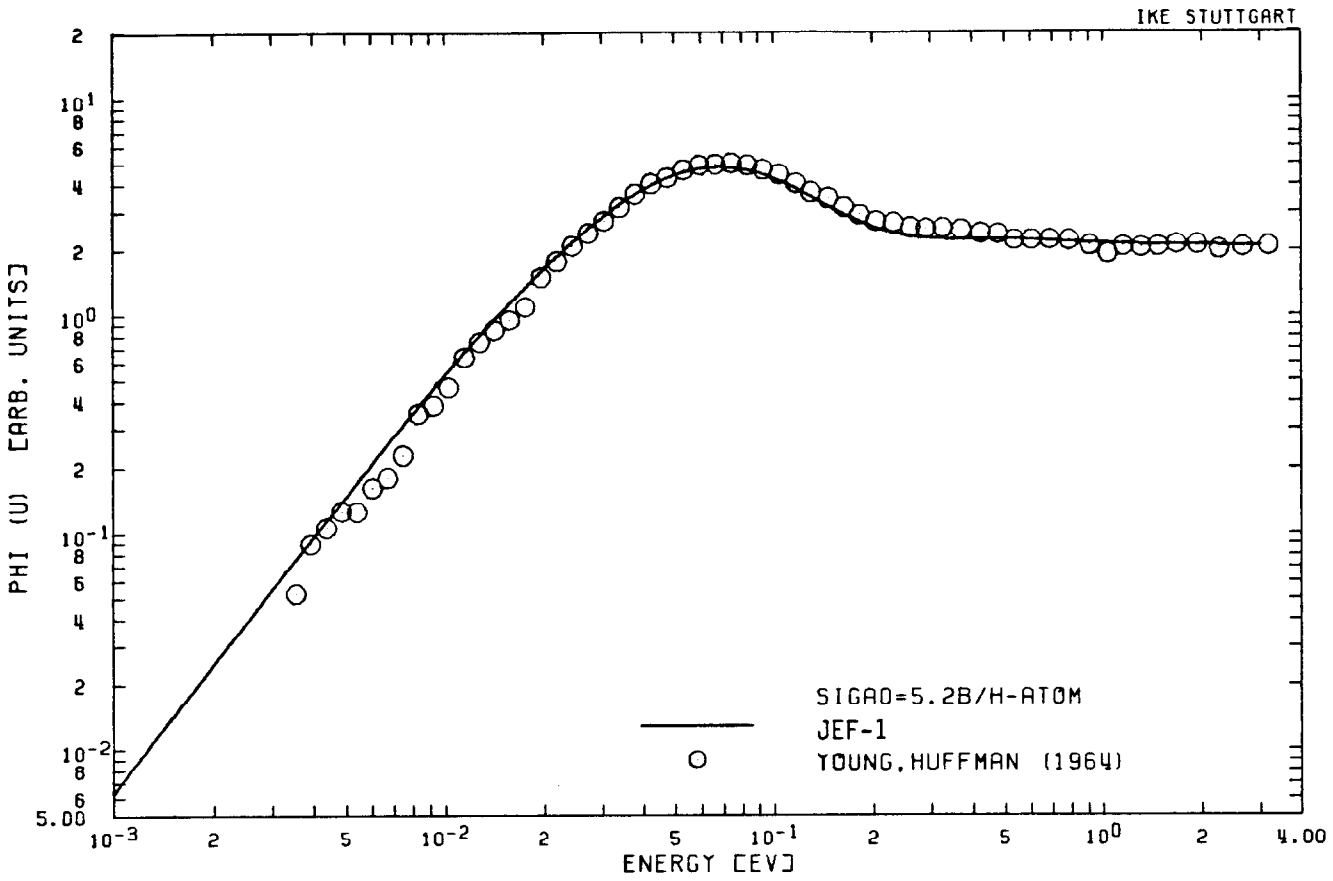

Fig. 4.3: Infinite medium neutron spectrum in borated water (H_2O) at room temperature

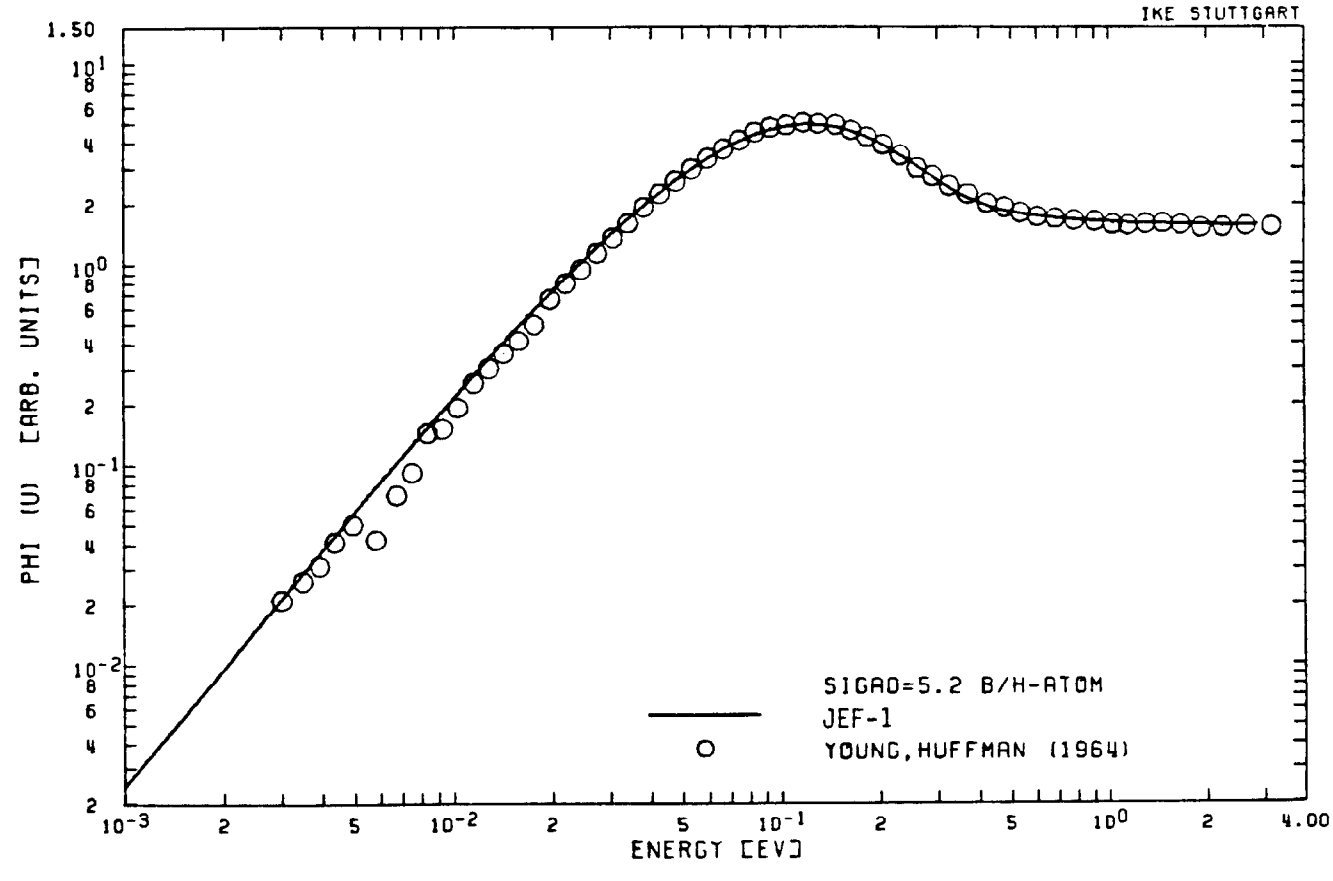

Fig. 4.4: Infinite medium neutron spectrum in borated water (H_2O) at T = 316 C

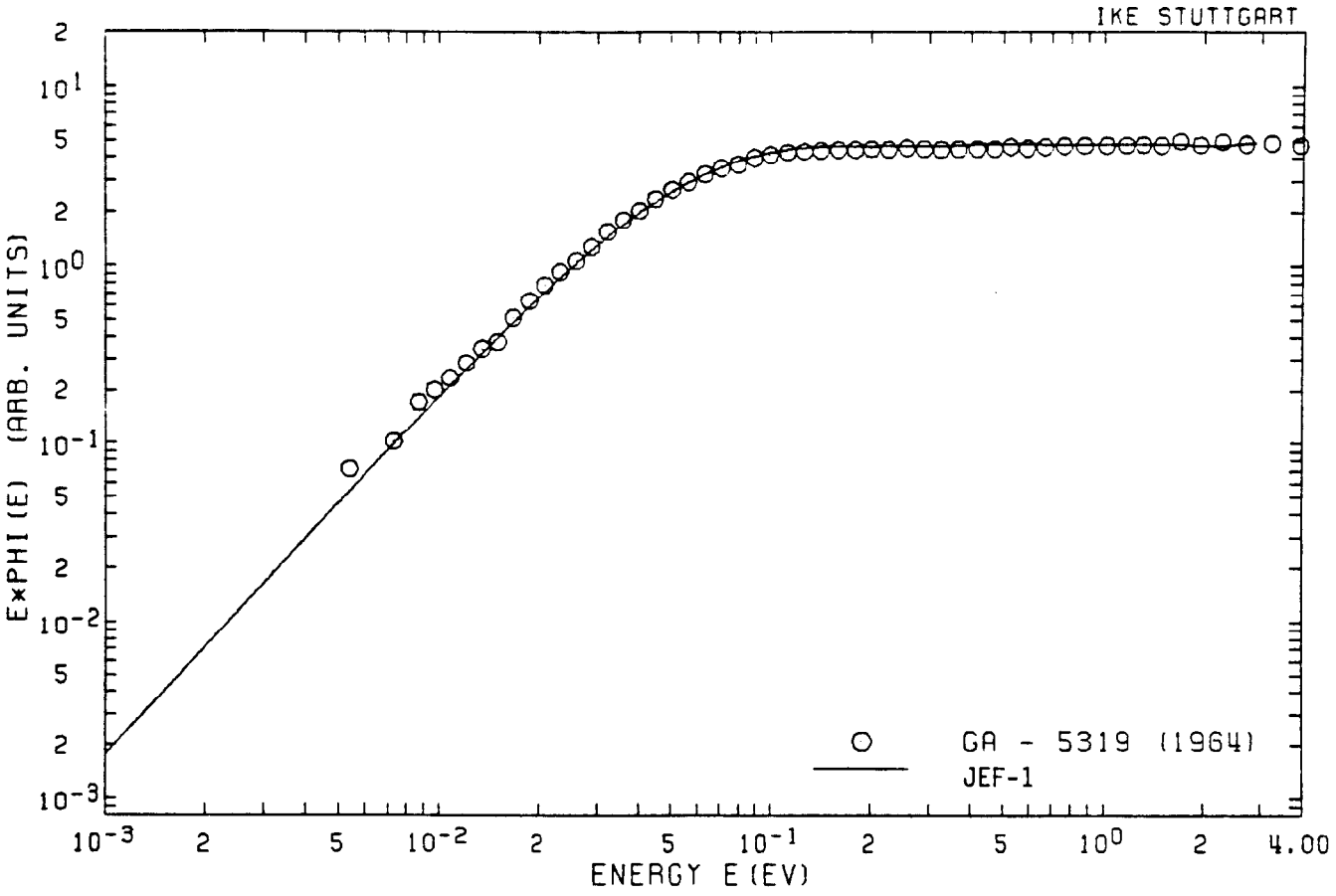

Fig. 4.5: Neutron spectrum in borated D_2O at room temperature (2.1 b/D-atom)

4.2 Thermal Reactor Benchmarks

For each of the analysed systems JEF-1 results are presented together with results of ENDF/B (version IV and/or V) essentially from /3/ and results of IKE calculations with ENDF/B data as well as the corresponding experimental values. The definitions of cell reaction rate ratios measured at several experiments are given in Table 4.1.

Table 4.1: Definitions of cell reaction rate ratio parameters

Parameter	Definition
ρ^{28}	epithermal/thermal U-238 captures
δ^{25}	epithermal/thermal U-235 fissions
δ^{28}	U-238 fissions / U-235 fissions
C^{*}	U-238 captures / U-235 fissions
δ^{49}	epithermal/thermal Pu-239 fissions
ε^{25}_{49}	U-235 fissions / Pu-239 fissions

4.2.1 Homogeneous U-235/H_2O Assemblies

The CSEWG benchmarks (ORNL-1 through 4 and 10) were analysed by the RSYST/CGM program system for both, JEF-1 and ENDF/B data. Calculated k_{eff} results are given in Tab. 4.2. In this table average values of results of different institutions for ENDF/B-IV and for ENDF/B-V are given too. The JEF-1 results ($\langle k_{eff} \rangle$, averaged over all ORNL assemblies, is 0.9996 ± 0.0015) agree well with the experimental values as it is the case for ENDF/B-IV ($\langle k_{eff} \rangle$ = 0.9985 ± 0.0017) and ENDF/B-V ($\langle k_{eff} \rangle$ = 1.0002 ± 0.0023). The average (corrected) experimental $\langle k_{eff} \rangle$ is 0.9990 ± 0.0005. The JEF-1 results were obtained by a 60 groups calculation in S_8/P_3-approximation. The corresponding RSYST/CGM calculations based on ENDF/B-IV, -V were performed with S_4/P_1 and 18 groups. The JEF-1 results are consistent to the ENDF/B-V results /3/. An overview of calculated and measured k_{eff}-values versus the H/U-235 atomic ratio is represented in Fig. 4.6. All results (JEF-1 and ENDF/B) show a good agreement with the experiment. For completeness the benchmarks for homogeneous uranyl nitrate solutions should be extended to assemblies with higher and lower H/U-235 ratios as it has been done in /3/ for ENDF/B-V (e. g. Gwin-Magnuson criticals).

4.2.2 TRX Assemblies 1 through 4

The TRX-benchmarks are very sensitive to the treatment of the resolved resonance region. For the TRX-1 and TRX-2 experiments k_{eff} and the lattice cell reaction rate ratios ρ^{28}, δ^{25}, C* and δ^{28} as well as fast advantage factors and thermal activation disadvantage factors were measured. TRX-3 and TRX-4 are two-zone cores with a tight (V_{mod}/V_{fuel} = 1) and a wide (V_{mod}/V_{fuel} = 8) lattice surrounded by a driver zone with a UO_2 lattice.

Table 4.2: Calculated k_{eff} for U-235-H_2O benchmarks

Assembly I.D.	H/U-235 Ratio	ENDF/B-IV,V RSYST/CGM	JEF-1 RSYST/CGM	ENDF/B-IV ref. /3/	ENDF/B-V (ENDF-311)
ORNL- 1	1378	1.0018	1.0013	1.0005±0.0014	1.0025±0.0019
ORNL- 2	1177	1.0009	1.0015	1.0006±0.0009	1.0020±0.0023
ORNL- 3	1033	0.9985	0.9985	0.9970±0.0015	0.9972±0.0022
ORNL- 4	972	1.0001	0.9997	0.9982±0.0013	1.0016±0.0022
ORNL-10	1835	0.9987	0.9986	0.9964±0.0022	0.9977±0.0020

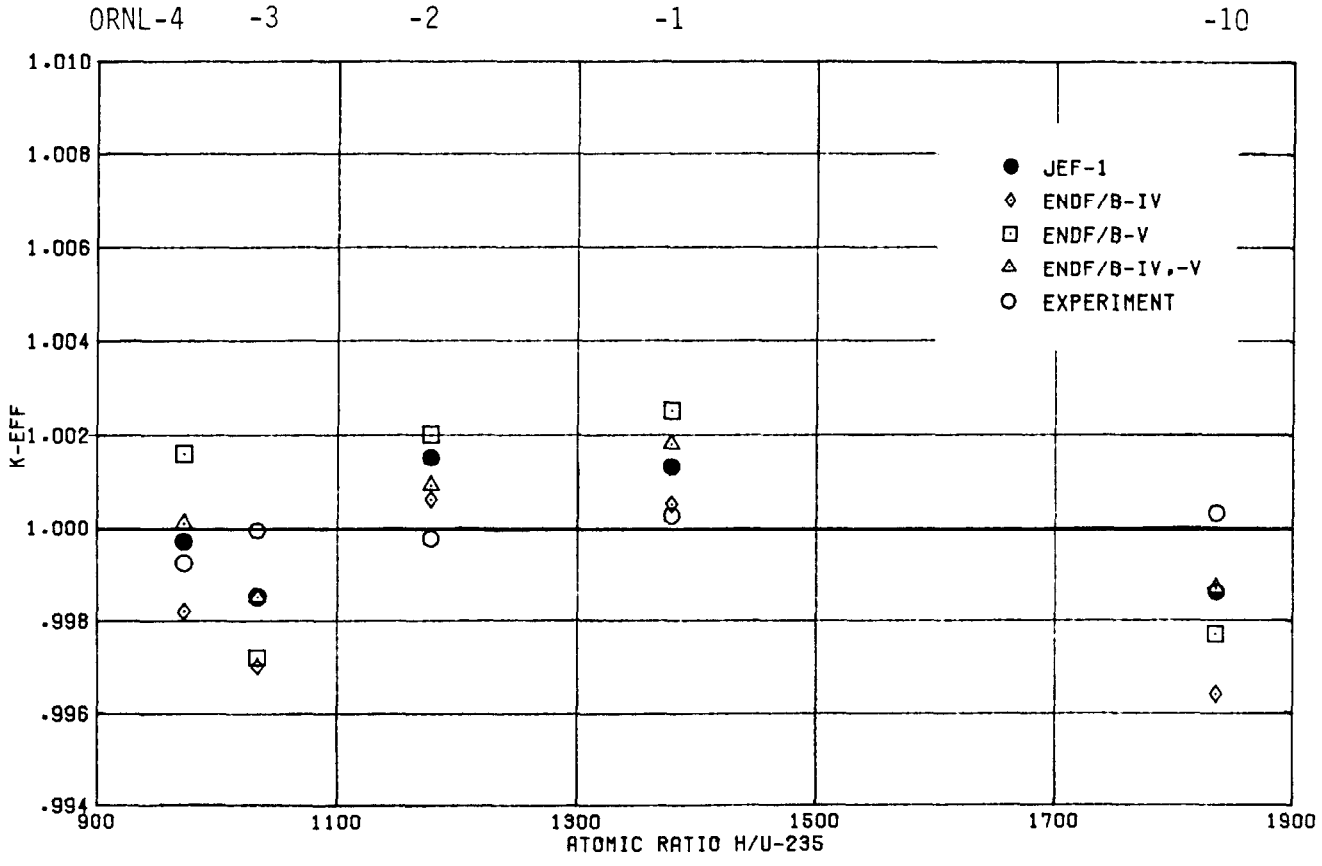

Fig. 4.6: k_{eff} versus the H/U-235 atomic ratio for homogeneous U-235-H_2O benchmarks (ORNL)

Results from RSYST/CGM calculations based on JEF-1 together with ENDF/B-IV and ENDF/B-V results from Ref. /3/ are given in Table 4.3 for TRX-1 and Table 4.4 for TRX-2, respectively. These assemblies were calculated by a fine discretization for the space-dependent spectral calculation and an appropriate weighting function (NR-approximation) for multigroup data in the unresolved/resolved resonance range of U-238. Thus a fairly good agreement between calculated and measured k_{eff}-values and reaction rate ratios could be achieved. The values are very close to those calculated with ENDF/B-V. A remarkable improvement of the epithermal/thermal U-238 capture ratio and k_{eff} could be found compared to the ENDF/B-IV calculations. In addition, for TRX-1 and TRX-2 cell fast advantage factors calculated by JEF-1 and ENDF/B-IV /17/ are listed in Table 4.5. For both the U-238-fission and the Al(n,α)-reaction calculation and measurement agree within the experimental uncertainty. Thermal activation disadvantage factors for the nuclides U-235, Dy-164 and Lu-176 are listed in Table 4.6. The JEF-1 results (but also ENDF/B-IV) agree well with corresponding measurements.

For the TRX-3 and TRX-4 benchmarks the results of integral parameters based on JEF-1 and taken from ref. /18, 19/ are listed in Table 4.7 and 4.8, respectively. As in the case for TRX-1 and -2 the JEF-1 epithermal/thermal U-238 capture ratio and k_{eff} agree remarkably better to the experimental values than corresponding ENDF/B-IV results (no ENDF/B-V results were found for these benchmarks). Regarding the calculated k_{eff}values for TRX-1 through -4 (Fig. 4.7) together with the corresponding epithermal/thermal U-238 capture ratio (ρ^{28}, Fig. 4.8) we can summarize as follows:

- k_{eff}, averaged over TRX-1 through TRX-4 from calculations based on different evaluated nuclear data libraries:

  - JEF-1 : $\langle k_{eff} \rangle$ = 0.9981 ± 0.0021
  - ENDF/B-V : $\langle k_{eff} \rangle$ = 0.9973 ± 0.0016 (averaged only over TRX-1 and -2)
  - ENDF/B-IV : $\langle k_{eff} \rangle$ = 0.9914 ± 0.0029.

  It is evident, that JEF-1 and ENDF/B-V data lead to a comparable accuracy in calculating k_{eff} for TRX-lattices. Regarding Fig. 4.8 one can see that ρ^{28} increases strongly if the lattice becomes tighter. However, the discrepancies of measured and calculated ρ^{28}-values have a maximum (see C/E in Fig. 4.8) at the volume ratio V_{mod}/V_{fuel} = 2.35 (TRX-1). It may be that some errors in resolved and unresolved resonance range will be compensated.

Table 4.3: Integral parameters for TRX-1

Parameter	Experiment	Calculation		
		JEF-1 RSYST/CGM	ENDF/B-IV ref. /3/ (ENDF-311)	ENDF/B-V
ρ_{28}	1.320 ±0.021	1.3569	1.382 ±0.006	1.359
δ_{25}	0.0987±0.0010	0.0992	0.0994±0.0005	0.1003
δ_{28}	0.0946±0.0041	0.1001	0.0955±0.0006	0.0989
C^*	0.797 ±0.008	0.7984	0.806 ±0.002	0.798
k_{eff}	1.0000	0.9960	0.9876±0.0032	0.9961

Table 4.4: Integral parameters for TRX-2

Parameter	Experiment	Calculation		
		JEF-1 RSYST/CGM	ENDF/B-IV ref. /3/ (ENDF-311)	ENDF/B-V
ρ_{28}	0.837 ±0.016	0.8374	0.863 ±0.005	0.846
δ_{25}	0.0614±0.0008	0.0608	0.0609±0.0003	0.0614
δ_{28}	0.0693±0.0035	0.0714	0.0676±0.0003	0.0699
C^*	0.647 ±0.006	0.6393	0.647 ±0.002	0.642
k_{eff}	1.0000	0.9973	0.9935±0.0031	0.9984

Table 4.5: Cell fast advantage factors for TRX-1 and TRX-2

Reaction	Lattice	Experiment	JEF-1 CGM	ENDF/B-IV RSYST1 /17/
U-238-fission	TRX-1	1.145±0.028	1.126	1.130
	TRX-2	1.23 ±0.03	1.215	1.216
Al(n,α)	TRX-1	-	1.104	1.101
	TRX-2	1.21 ±0.04	1.176	1.171

Table 4.6: Thermal activation disadvantage factors for TRX-1 and TRX-2

Nuclide	Lattice	Experiment	JEF-1 CGM	ENDF/B-IV RSYST1 /17/
U-235	TRX-1	1.317±0.013	1.313	1.302
	TRX-2	1.378±0.013	1.367	1.365
Dy-164	TRX-1	1.302±0.013	1.310	1.300
	TRX-2	1.360±0.008	1.364	1.361
Lu-176	TRX-1	1.200±0.011	1.195	1.182
	TRX-2	1.236±0.011	1.232	1.221

Table 4.7: Integral parameters for TRX-3

Parameter	Experiment	Calculation	
		JEF-1 RSYST/CGM	ENDF/B-IV ref. /18, 19/
ρ_{28}	3.03 ± 0.05	3.013	3.07
δ_{25}	0.231 ± 0.003	0.236	0.235
δ_{28}	0.167 ± 0.008	0.1725	0.174
C^*	1.255 ± 0.011	1.2402	1.252
k_{eff}	1.0	1.0010	0.9908±0.0039

Table 4.8: Integral parameters for TRX-4

Parameter	Experiment	Calculation	
		JEF-1 RSYST/CGM	ENDF/B-IV ref. /18, 19/
ρ_{28}	0.481 ± 0.011	0.4760	0.491
δ_{25}	0.0358± 0.0005	0.0344	0.0345
δ_{28}	0.0482± 0.0020	0.0473	0.0467
C^*	0.531 ± 0.004	0.5244	0.527
k_{eff}	1.0	0.9979	0.9937±0.0053

- ENDF/B-IV underpredicts k_{eff} and overpredicts epithermal U-238 capture.

- For TRX-1 the JEF-1 and ENDF/B-V results for the epithermal/thermal U-238 capture ratio overpredict the experimental values, so that k_{eff} for TRX-1 is not as accurate as for TRX-2 through TRX-4. Results for TRX-3 and TRX-4, however, are influenced from the UO_2 driver lattice; the agreement with experimental values may be due to the general good agreement of theory and experiment for UO_2-lattices (see also results for BAPL-UO_2 and HI-C benchmarks).

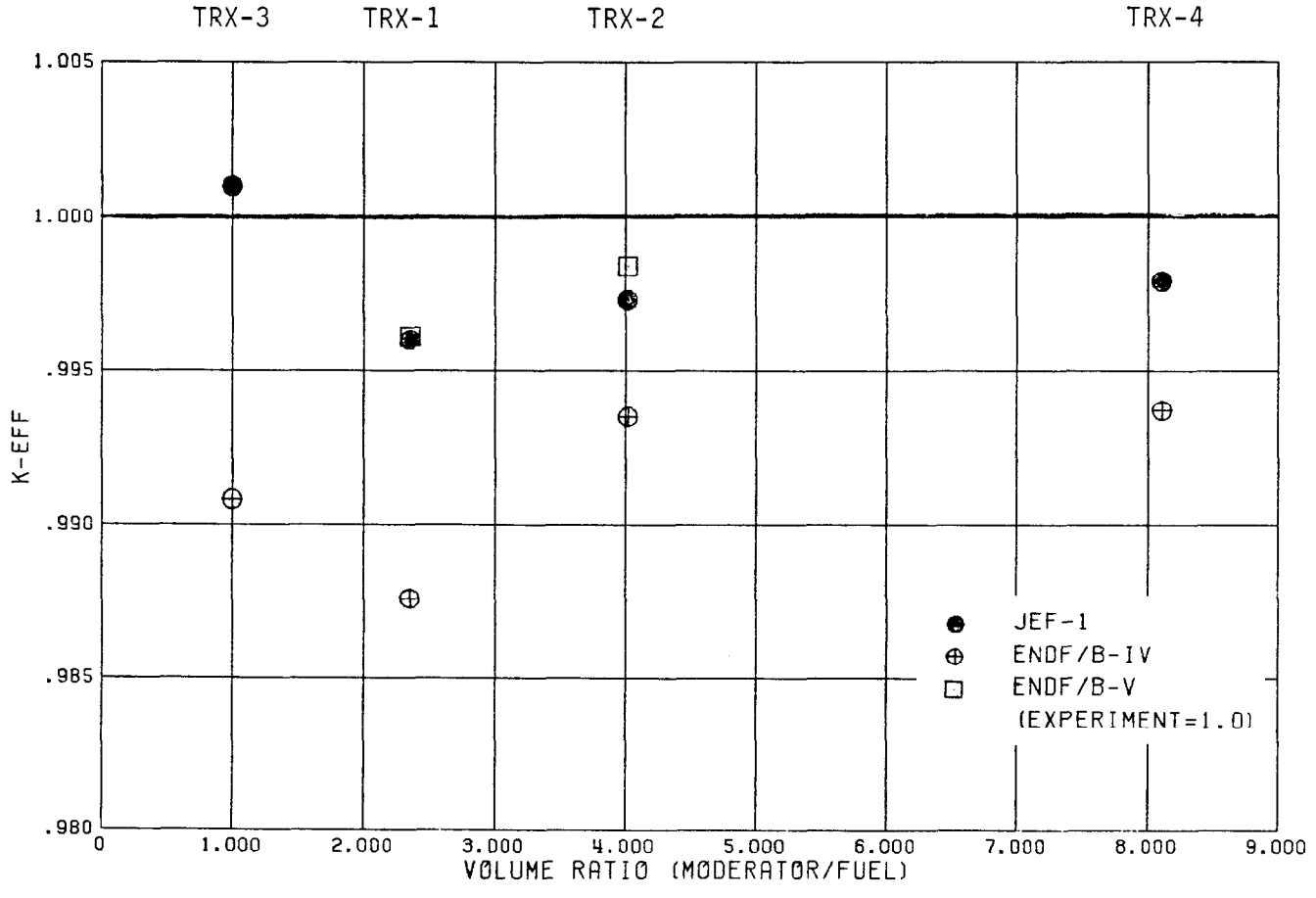

Fig. 4.7: k_{eff} for the uranium metal lattices TRX-1 through -4

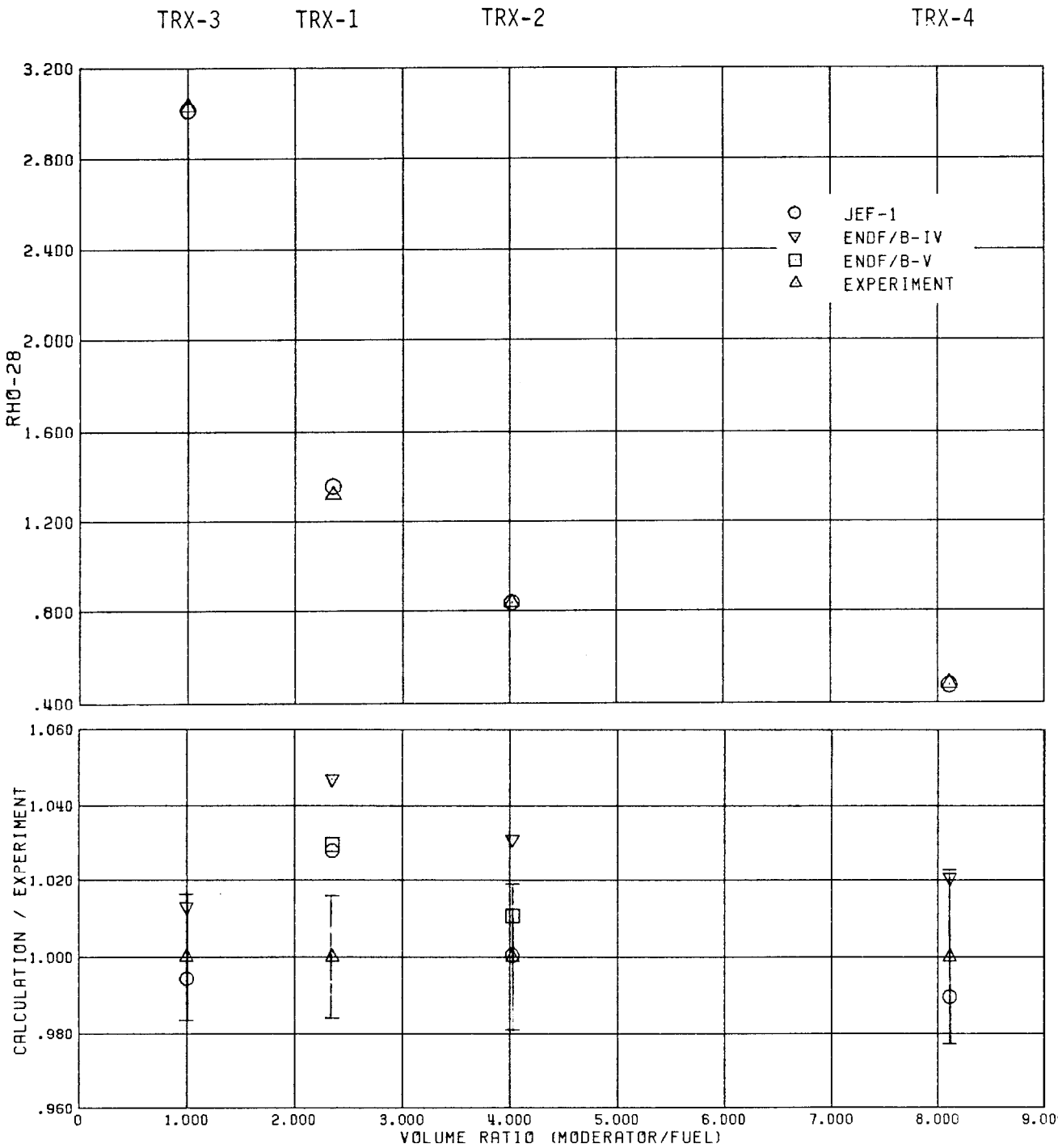

Fig. 4.8: ρ^{28} and C/E quota of ρ^{28} for the uranium metal lattices TRX-1 through TRX-4 as a function of moderator/fuel volume ratio

4.2.3 BAPL-UO_2-Benchmarks 1, 2, and 3

For the BAPL-UO_2-1, -2, and -3 benchmarks integral parameters as described for TRX are measured. Fast advantage factors, however, are not available.

Tables 4.9 through 4.12 contain RSYST/CGM results based on JEF-1 and ENDF/B-IV/-V together with published results /3, 20/ based on ENDF/B-IV and ENDF/B-V. The RSYST/CGM calculations based on JEF-1 agree very well with the measured integral parameters except the epithermal/thermal U-238 capture ratio for BAPL-UO_2-2. The average k_{eff}-values for the three benchmarks and different evaluated data libraries are:

JEF-1: $\langle k_{eff} \rangle = 0.9996 \pm 0.0007$

ENDF/B-V: $\langle k_{eff} \rangle = 1.0036 \pm 0.0008$

ENDF/B-IV: $\langle k_{eff} \rangle = 0.9929 \pm 0.0013$

The RSYST/CGM-results based on ENDF/B-IV,-V (data partly from ENDF/B-IV and - if available - from ENDF/B-V) are not as accurate as JEF-1. These calculations, however, were performed using a non-exactly interpolated σ_0-value for U-238 in the NR-weigthing function.

The ENDF/B-IV values are too low as in the case of TRX. This corresponds obviously to the too high epithermal/thermal U-238 capture ratios (see Tables 4.9 through 4.11). The calculated U-235 thermal activation disadvantage factors (Table 4.12) for JEF-1 (and ENDF/B-IV) agree sufficiently well with measured values.

Table 4.9: Integral parameters for BAPL-UO_2-1

Parameter	Experiment	Calculation			
		ENDF/B-IV,V RSYST/CGM	JEF-1 RSYST/CGM	ENDF/B-IV ref. /3, 20/	ENDF/B-V ref. /3, 20/
ρ_{28}	1.39 ±0.01	-	1.4196	1.447	1.414
δ_{25}	0.084 ±0.002	-	0.0841	0.0841	0.0840
δ_{28}	0.078 ±0.004	-	0.0775	0.0738	0.0782
C^*	-	-	0.8130	0.822	0.810
k_{eff}	1.0000±0.00065	1.0050	1.0001	0.9914±0.0021	1.0030±0.0003

Table 4.10: Integral parameters for BAPL-UO_2-2

Parameter	Experiment	Calculation			
		ENDF/B-IV,V RSYST/CGM	JEF-1 RSYST/CGM	ENDF/B-IV ref. /3, 20/	ENDF/B-V ref. /3, 20/
ρ_{28}	1.12 ±0.01	-	1.1771	1.195	1.173
δ_{25}	0.068 ±0.001	-	0.0685	0.0683	0.0680
δ_{28}	0.070 ±0.004	-	0.0668	0.0633	0.0653
C^*	-	-	0.7393	0.745	0.738
k_{eff}	1.0000±0.00062	0.9978	0.9999	0.9932±0.0006	1.0033±0.0003

Table 4.11: Integral parameters for BAPL-UO_2-3

Parameter	Experiment	Calculation			
		ENDF/B-IV,V RSYST/CGM	JEF-1 RSYST/CGM	ENDF/B-IV ref. /3, 20/	ENDF/B-V ref. /3, 20/
ρ_{28}	0.906 ±0.010	-	0.9201	0.944	0.914
δ_{25}	0.052 ±0.001	-	0.0526	0.0523	0.0525
δ_{28}	0.057 ±0.003	-	0.0549	0.0518	0.0533
C^*	-	-	0.6591	0.667	0.656
k_{eff}	1.0000±0.0005	0.9974	0.9988	0.9940±0.0015	1.0045±0.0014

Table 4.12: U-235 thermal activation disadvantage factors for the BAPL-UO_2 assemblies

Assembly	Experiment	JEF-1 (CGM)	ENDF/B-IV (RSYST1) /17/
BAPL-UO_2-1	1.10 ± 0.01	1.0974	-
-2	1.13 ± 0.01	1.1051	1.14
-3	1.13 ± 0.01	1.1163	-

4.2.4 HI-C-Benchmarks-3, 10, 11, and 13

For the considered HI-C assemblies results for the effective multiplication factor k_{eff} are given in Table 4.13. RSYST/CGM-results based on JEF-1 and some results from Ref. /20/ and /21/ for comparison are listed in these figures. The JEF-1 results agree well with the experiment (average k_{eff}: 1.0004 ± 0.0010) and have no significant deviation, even if the H/U-238 ratio changes remarkably from 4.15 to 1.32. However, the agreement could only be reached by using correct weighted cross-sections in the resonance and fast energy region (σ_0-interpolation and multi-zone model for resonance calculation). The ENDF/B-V results from Ref. /20/ show a stronger deviation between the different benchmarks (average value 1.0012 ± 0.0040, averaged over HI-C-10, -11 and -13). This may be influenced by the spectral calculation methods rather than by the ENDF/B-V-data, however.

The strong differences in the neutron spectra between HI-C-3 and HI-C-13 are shown in Fig. 4.9. It is obvious, that the spectral calculations for the lattice cell must be performed very carefully not only in the thermal and resolved energy range but also in the range of the unresolved resonances (above 4 keV). In RSYST/CGM this is realized using the NR-approximation with a heterogeneity correction for the lattice.

4.2.5 SHERWOOD Assembly Capture Reaction Rates for Actinides

The actinide reaction rates measured in the SHERWOOD assembly (5 x 5 PWR fuel rods of a typical PWR 17 x 17 assembly) were transposed and corrected for the case of an infinite lattice of this fuel type /12/. An exact definition of the infinite lattice which should represent a typical PWR reactor, however, was not given, so that the calculated values based on JEF-1 may not be quite representative. The calculated and measured data are listed in Table 4.14. Nevertheless, it can be seen that the agreement of experiment and calculation is rather good for U-238, Pu-239 and Pu-240. For Pu-241, Pu-242, Am-241 and Am-243 deviations up to 14 % were found, which cannot be explained by a possible incorrect description of the PWR-lattice alone. The reaction rates presented in Table 4.14 are normalized to the fission rate of U-235. The average of the calculated and measured reaction rate ratios (C/E) is 0.976 ± 0.072.

Table 4.13: Calculated k_{eff} for HI-C benchmark experiments

Assembly	H/U-238	JEF-1	KfK ref. /21/	ENDF/B-V ref. /20/
HIC- 3	4.15	1.0015	-	-
HIC-10	2.91	0.9999	0.9968±0.0152	1.0041
HIC-11	2.29	1.0010	-	1.0029
HIC-13	1.32	0.9994	-	0.9966

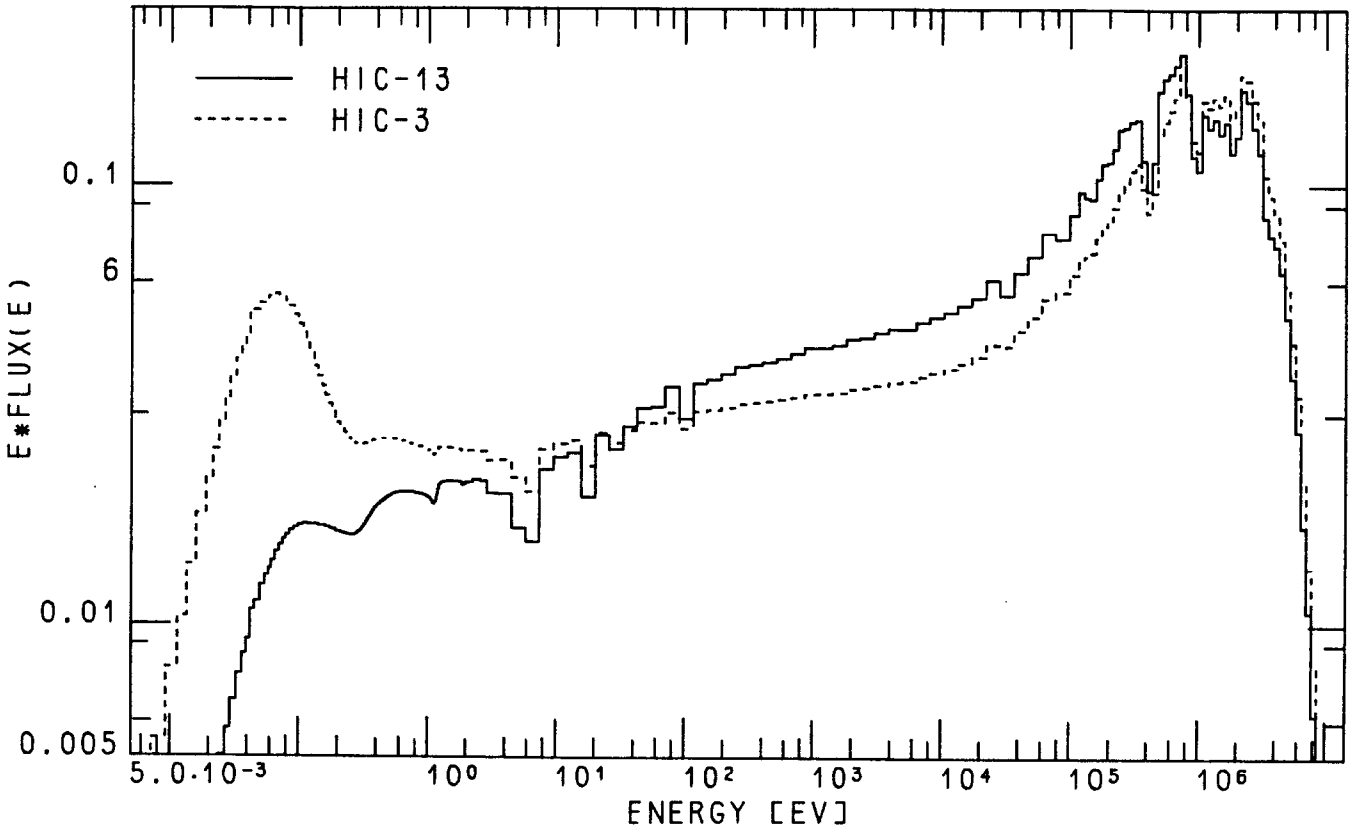

Fig. 4.9: Comparison of cell-spectra for a wide (HI-C-3) and tight lattice (HI-C-13)

Table 4.14: Capture reaction rates for actinides measured in SHERWOOD assembly /12/ (irradiated in MELUSINE reactor Grenoble/France) normalized to the fission rate of U-235

Reaction Rate	Experiment	Calculation JEF-1	C/E
U-235 Absorption	1.233 ±0.017	1.224	0.993
U-235 Capture	0.233 ±0.003	0.224	0.961
U-238 Capture	0.01917±0.00014	0.0199	1.037
Pu-239 Capture	1.508 ±0.010	1.484	0.984
Pu-240 Capture	5.1 ±0.075	5.228	1.025
Pu-241 Capture	1.022 ±0.029	0.919	0.900
Pu-242 Capture	0.604 ±0.016	0.661	1.094
Am-241 Capture	3.185 ±0.065	2.762	0.867
Am-243 Capture	1.248 ±0.025	1.148	0.920

4.2.6 Summary for Uranium Lattices

For the different low enriched uranium/uranium oxide lattices analysed with data based on JEF-1 the percentage deviation of calculated and measured integral parameters are listed in Table 4.15. The largest deviation in k_{eff} was found for TRX-1 (-0.40 %). For the uranium oxide lattices the agreement of all analysed cores was better than 0.2 %.

For the following assemblies reaction rate ratios as ρ^{28}, δ^{25}, δ^{28} and C* (measured only for the TRX- and BAPL-benchmarks) show deviations larger than the experimental uncertainty:

- TRX-1: ρ^{28}, δ^{28}
- TRX-2: C*
- TRX-3: δ^{25}, C*
- TRX-4: δ^{25}, C*
- BAPL-UO_2-1, -2, and -3: ρ^{28} (BAPL-UO_2-2: > 5 %)

The multiplication factors k_{eff} based on JEF-1 are plotted in Fig. 4.10 for all uranium lattice benchmarks as a function of the moderator/fuel volume ratio. It seems that there is a slight tendency for higher k_{eff}-values at lower moderator/fuel volume ratios. The small number of different experiments analysed here, however, cannot give a representative picture.

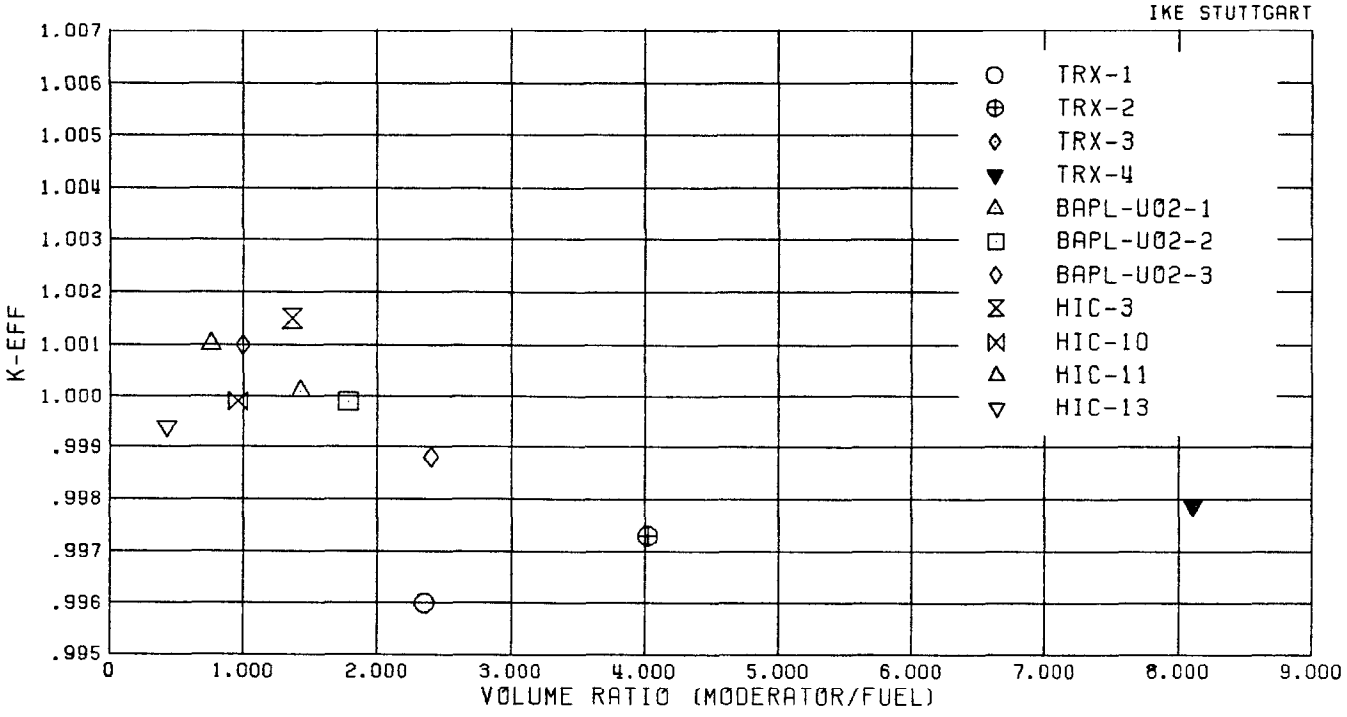

Fig. 4.10: k_{eff} for uranium lattice benchmarks calculated with JEF-1

Table 4.15: Percentage deviation of JEF-1 results from experiment for uranium benchmarks

Assembly	Parameter				
	ρ^{28}	δ^{25}	δ^{28}	C*	k_{eff}
TRX-1	2.80 (1.59) *	0.51 (1.01) *	5.81 (4.33) *	0.18 (1.00) *	-0.40
TRX-2	0.05 (1.91) *	-0.98 (1.30) *	3.03 (5.05) *	-1.19 (0.93) *	-0.27
TRX-3	-0.56 (1.65) *	2.16 (1.30) *	3.29 (4.79) *	-1.18 (0.88) *	0.10
TRX-4	-1.04 (2.29) *	-3.91 (1.40) *	-1.87 (4.15) *	-1.24 (0.75) *	-0.21
BAPL-UO_2-1	2.13 (0.72) *	0.12 (2.38) *	-0.64 (5.13) *	-	0.01 (0.07) *
BAPL-UO_2-2	5.10 (0.89) *	0.74 (1.47) *	-4.57 (5.71) *	-	-0.01 (0.06) *
BAPL-UO_2-3	1.56 (1.10) *	1.15 (1.92) *	-3.68 (5.26) *	-	-0.12 (0.05) *
HI-C-3					0.15
HI-C-10					0.01
HI-C-11					0.10
HI-C-13					0.01

* experimental uncertainty

4.2.7 Homogeneous $Pu-H_2O$-Systems

- Infinite Solution

For an infinite homogeneous critical solution of Pu-239 in water /14/ with an H/Pu atom ratio of 3694.5 the JEF-1 result for k_∞ was 0.9957. For comparison, the average k_∞ based on ENDF/B-IV is 0.9942±0.0004 (average of different calculations), and 0.9999±0.0014 for ENDF/B-V (LANL-calculations). The ENDF/B-results are given in ENDF-311 /3/. The JEF-1 result for k_∞ lies 0.42 % lower than the corresponding ENDF/B-V result from LANL. A reason may be that for Pu-239 the average number of neutrons per thermal fission ($\bar{\nu}$) is higher in ENDF/B-V than in JEF-1. Taking into account for JEF-1 the modified energy dependent $\bar{\nu}_p$ for Pu-239 given in /22/ k_∞ becomes 0.9970 which lies just within the 2σ-bounds of the LANL/ENDF/B-V calculation. But also the modified $\bar{\nu}$ is smaller than that from ENDF/B-V. If the fission yield $\bar{\nu}$ from ENDF/B-V (which is constant in the thermal and epithermal energy range) is used instead of that from JEF-1 the average k_∞ for the critical solution is 1.0021.

- PNL-1 through 8, and 12

For the analysed homogeneous $Pu-H_2O$ assemblies the calculated k_{eff} are given in Table 4.16 and plotted in Fig. 4.11 where our results with JEF-1 and ENDF/B-IV,-V data are compared with those from /3/ for ENDF/B-IV and -V.

The agreement of calculations for PNL-1 through 8 and 12 with the corresponding experimental values is relatively poor, the only exception is PNL-3. For the bare spheres (PNL-1 through 6) it seems that the agreement with the experiment is better for high H/Pu ratios. For a reflected sphere (PNL-12) with about the same high H/Pu ratio than PNL-3, however, the calculated k_{eff} is too high again (> 1 %). Generally, for the PNL-benchmarks the JEF-1 results are comparable to those from ENDF/B-V. The average of the k_{eff} values for the nine assemblies from calculations based on following data libraries are:

JEF-1 : $\langle k_{eff} \rangle = 1.0123 \pm 0.0066$,
ENDF/B-IV, V : $\langle k_{eff} \rangle = 1.0111 \pm 0.0072$ (results of calculations at IKE),
ENDF/B-IV : $\langle k_{eff} \rangle = 1.0142 \pm 0.0066$ (ref. /3/),
ENDF/B-V : $\langle k_{eff} \rangle = 1.0115 \pm 0.0063$ (ref. /3/).

Since all data from different sources yielded nearly the same discrepancies it is thought that not only data uncertainties but also systematic errors in the benchmark specifications are the cause of deviations between experiment and calculation /3, 23/.

Table 4.16: Calculated k_{eff} for Pu-H_2O benchmark experiments

Assembly I.D.	H / Pu Ratio	ENDF/B-IV,V RSYST/CGM	JEF-1 RSYST/CGM	ENDF/B-IV ref. /3/	ENDF/B-V (ENDF-311)
PNL- 1	668	1.0162	1.0176	1.0215±0.0039	1.0211±0.0021
PNL- 2	125	1.0103	1.0167	1.0185±0.0082	-
PNL- 3	1154	0.9961	0.9978	1.0002±0.0024	1.0003±0.0023
PNL- 4	873	1.0039	1.0060	1.0089±0.0026	1.0072±0.0023
PNL- 5	554	1.0093	1.0117	1.0147±0.0044	1.0110±0.0024
PNL- 6	125	1.0130	1.0165	1.0137±0.0032	1.0097±0.0030
PNL- 7	980	1.0174	1.0126	1.0141±0.0034	1.0151±0.0035
PNL- 8	758	1.0161	1.0175	1.0210±0.0029	1.0162±0.0038
PNL-12	1067	1.0175	1.0139	1.0156±0.0045	1.0110±0.0032

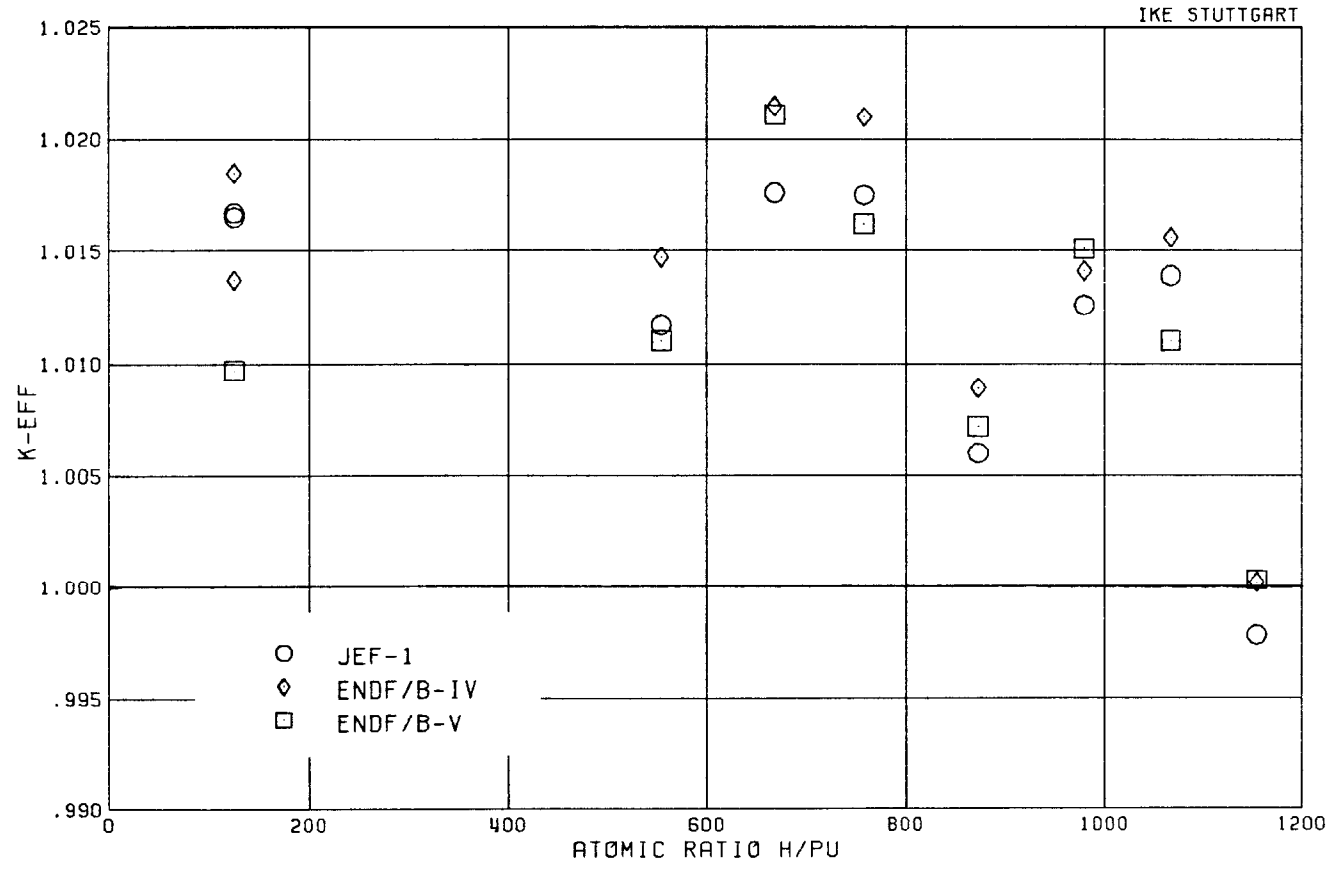

Fig. 4.11: k_{eff} versus the H/Pu atomic ratio for homogeneous Pu-H_2O benchmarks (PNL)

4.2.8 Mixed Oxide Benchmarks (PNL-30 through 35)

Results for the considered mixed oxide UO_2-PuO_2 benchmarks are listed in Table 4.17 for k_{eff} and in Table 4.18 for k_∞ and calculated lattice cell reaction rate ratios. The overall agreement of experimental k_{eff} with results from JEF-1 data is satisfying and is comparable to the ENDF/B-V results /3, 24/. This also holds for the calculated integral parameters of Table 4.18, where the maximum deviation of the results based on JEF-1- and on ENDF/B is less than 0.8 % for k_∞ and a few percent for cell reaction rate ratios (the greatest deviation was found for δ^{28}).

The calculated values of k_{eff} are plotted in Fig. 4.12. As for the uranium lattices, the values based on ENDF/B-IV are lower than the corresponding values based on ENDF/B-V and JEF-1, respectively. For non-poisoned systems it seems that the calculated k_{eff}-values increase for higher moderator to fuel volume ratios. For poisoned systems a maximum between V_{H_2O}/V_{fuel} = 2.50 and 3.00 is observed (see Fig. 4.12) for JEF-1. However, there are too few values to see a clear tendency.

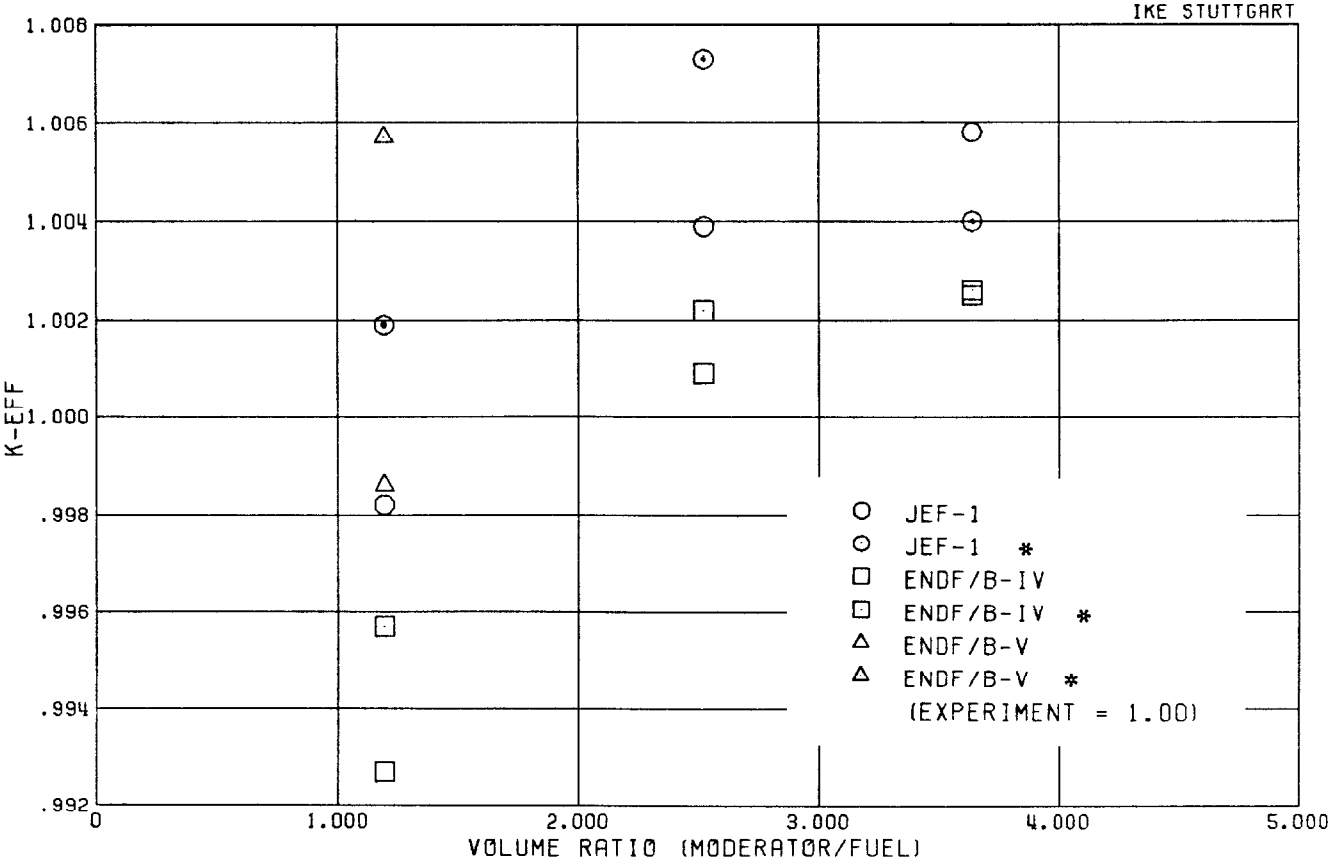

Fig. 4.12: k_{eff} for the CSEWG mixed U-Pu-oxide benchmarks
(UO_2+2wt% PuO_2; 8 % Pu-240) * boron poisoned

Table 4.17: k_{eff} for the mixed U-Pu-oxide benchmarks PNL-30 through 35 (UO_2-2 wt% PuO_2; 8 % Pu-240)

Lattice	Pitch (cm)	Water/Fuel Volume Ratio	Critical No. of Rods	Boron Concen-tration (wppm B)	JEF-1 (RSYST/ CGM)	ENDF/B-IV ref. /3/	ENDF/B-V ref. /3, 24/
PNL-30	1.778	1.194	469	1.7±.1	0.9982	0.9927±0.0022	0.9986±0.0019
PNL-31			761	680.9±2	1.0019	0.9957±0.0021	1.0057±0.0019
PNL-32	2.209	2.524	195	0.9±1	1.0039	1.0009±0.0046	-
PNL-33			761	1090.4±2	1.0073	1.0022±0.0028	-
PNL-34	2.514	3.640	161	1.6±.1	1.0058	1.0025±0.0053	-
PNL-35			689	767.2±2	1.0040	1.0026±0.0032	-

Table 4.18: Comparison of calculated benchmark lattice parameters for some mixed oxide assemblies

Lattice	Data file	k_∞	ρ^{28}	δ^{25}	δ^{28}	C^*	δ^{49}	ϵ_{49}^{25}
PNL-31	JEF-1	1.2453	5.3468	.3237	.5073	3.3379	.1588	.2118
	ENDF/B-V *	1.25344	5.201	.322	.479	3.262	.156	.211
PNL-33	JEF-1	1.1719	2.6461	.1538	.3101	2.1592	.0860	.2217
	ENDF/B-V *	1.17872	2.602	.155	.298	2.131	.0851	.220
PNL-35	JEF-1	1.1467	1.8324	.1054	.2399	1.7373	.0627	.2300
	ENDF/B-V *	1.15508	1.800	.106	.231	1.717	.0620	.228

* results taken from /25/

4.2.9 D_2O Benchmarks MIT-1, 2, and 3

The lattice cell calculations for these benchmarks were performed with the system RSYST/CGM generating 60 energy group cross-sections for ANISN. Results for integral parameters (ρ^{28}, δ^{25}, δ^{28}, C*) and k_{eff} for an experimental buckling B_m^2 are given in the Tables 4.19 through 4.21 for MIT-1, 2 and 3.
k_{eff} based on JEF-1 and ENDF/B-IV are shown in Fig. 4.13 too.

The cell reaction rate ratios agree fairly well with the experimental values and seem to be better than results using ENDF/B-IV /18, 26/. Results based from ENDF/B-V are not known for these assemblies. There may be some doubt, if it is possible to get correct critical parameters using a simple energy-independent buckling for the cell-calculations.

The analysis of MIT-1 through 3 can be regarded only as a first step, for three experiments cannot give a reliable validation for D_2O-systems.

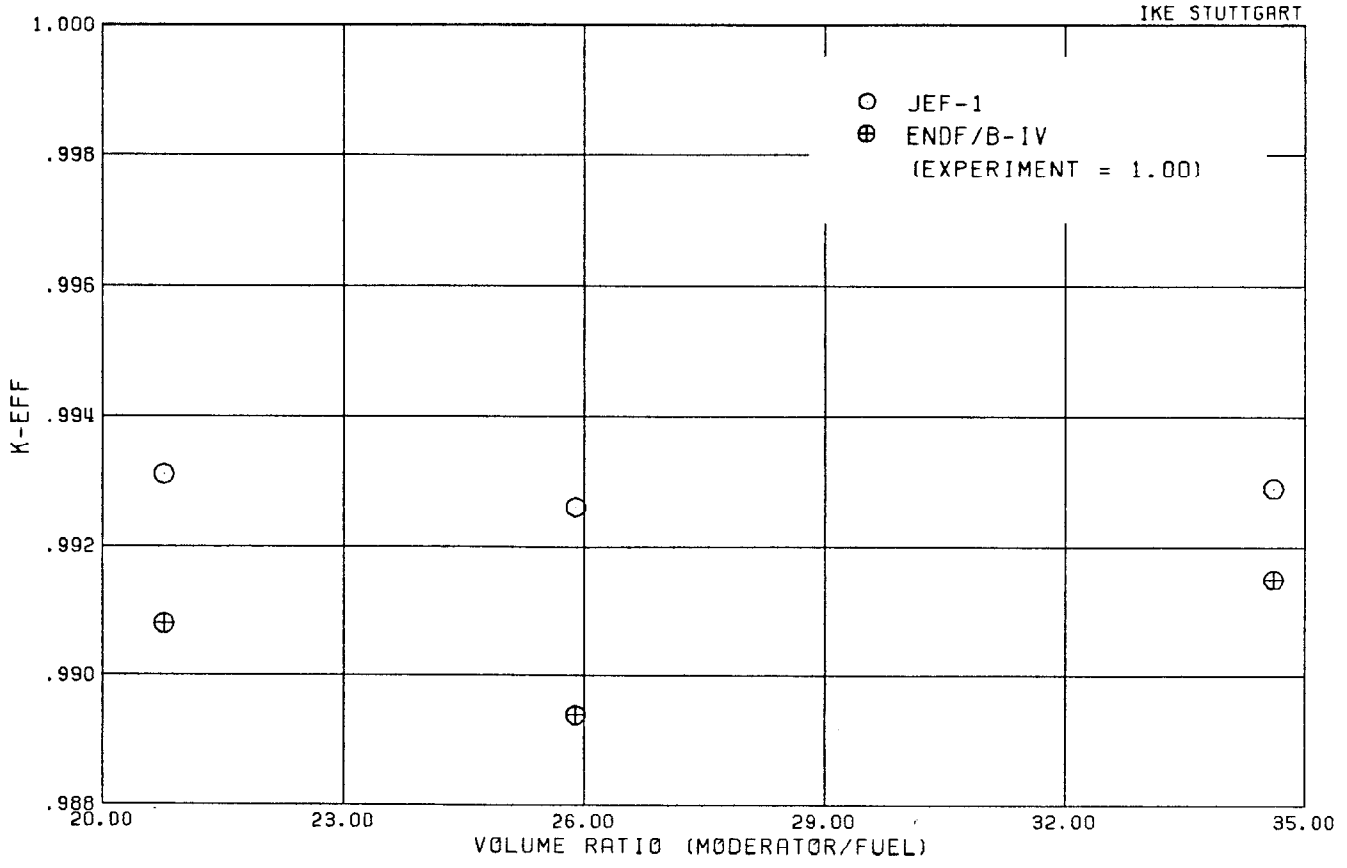

Fig. 4.13: k_{eff} for the CSEWG heavy water benchmarks MIT-1, 2, 3

Table 4.19: Integral parameters for the D_2O benchmark MIT-1

Parameter	Experiment	Calculation	
		JEF-1 CGM	ENDF/B-IV ref. /18, 26/
ρ^{28}	.502 ± .010	0.5162	0.51323
δ^{25}	.0469 ± .0019	0.0473	0.04291
δ^{28}	.0588 ± .0030	0.0607	0.061535
C^*	1.017 ± .023	0.9914	0.96084
k_{eff} (at given B_M^2)	1.0	.9931	0.9908±0.0004

Table 4.20: Integral parameters for the D_2O benchmark MIT-2

Parameter	Experiment	Calculation	
		JEF-1 CGM	ENDF/B-IV ref. /18, 26/
ρ^{28}	.400 ± .004	.4291	.42262
δ^{25}	.0335 ± .003	.0390	.038874
δ^{28}	.0587 ± .0030	.0597	.06001
C^*	.948 ± .020	.9394	.90830
k_{eff} (at given B_M^2)	1.0	.9926	.9894± .0004

Table 4.21: Integral parameters for the D_2O benchmark MIT-3

Parameter	Experiment	Calculation	
		JEF-1 CGM	ENDF/B-IV ref. /18, 26/
ρ^{28}	.313 ± .005	.3375	.32372
δ^{25}	.0265 ± .0011	.0304	.029824
δ^{28}	.0575 ± .0030	.0585	.057826
C^*	.859 ± .016	.8843	.85018
k_{eff} (at given B_m^2)	1.0	.9929	.9915± .0009

5 Conclusions

The excellent agreement of experimental and calculated parameters for different benchmark systems containing homogeneous solutions of U- and Pu-nitrate, heterogeneous assemblies of metallic uranium, uranium dioxide, mixed oxide, and heavy water moderated benchmarks demonstrate that calculations based on JEF-1 data are very reliable for thermal reactor applications.

As ENDF/B-V, for some assemblies JEF-1 data overpredict slightly the measured epithermal neutron capture in U-238 (see Fig. 4.8). This also holds for the ratio U-238 fissions/U-235 fissions (δ^{28}). This may be influenced by an overestimation of the U-238 fast fissions and/or by underestimated U-235 fissions. For all benchmarks, the choice of the fission spectra proved sensitive to the calculated parameters (e.g., $\Delta k \leq 0.002$ for uranium systems). The finite homogeneous Pu-systems show a deviation from up to 1.3 % against measurements which cannot be explained satisfactorily.

For further validation of the JEF-1 evaluated nuclear data file the list of benchmarks should be extended. For example, graphite moderated assemblies, ThO_2-systems or UO_2 benchmarks enriched at up to 3 - 4 % are of some interest.

References

/1/ Rowlands, J.L.; Tubbs, N.: The Joint Evaluated File: A New Nuclear Data Library for Reactor Calculations. A scientific collaboration between laboratories in Austria, France, F.R. Germany, Italy, Japan, Netherlands, Sweden, Switzerland, United Kingdom and the NEA Data Bank. Int. Conference on Nuclear Data for Basic and Applied Science, Santa Fé, 13.-17. May 1985

/2/ Index to the JEF-1 Nuclear Data Library. JEF Report 1,
Vol. 1: General Purpose File, NEA Data Bank (July 1985),
Vol. 2: Special Purpose File, NEA Data Bank (September 1985)

/3/ ENDF-311 Benchmark Data Testing of ENDF/B-V. BNL-NCS-31531 (1982)

/4/ Mac Farlane, R.E., et al.: The NJOY Nuclear Data Processing System. Volume I: User's Manual. LA-9309-M, Vol. 1, ENDF-324, 1982

/5/ Rühle, R.: RSYST, ein integriertes Modulsystem mit Datenbasis zur automatisierten Berechnung von Kernreaktoren. IKE 4-12 (1973)
Arshad, M.: Entwicklung und Verifikation eines Programmsystems zur Berechnung von Spektren und gewichteten Gruppenkonstanten für thermische und epithermische Spaltstoffsysteme. IKE 6-156 (April 1986)

/6/ Engle, W.W., jr.: A User's Manual for ANISN. K-1693 (1967)

/7/ Cross Section Evaluation Working Group Benchmark Specifications. ENDF-202 (Nov. 1974)

/8/ Boynton, A.R., et al.: High Conversion Critical Experiments. ANL-7203 (Jan. 1967)

/9/ Young, J.C.; Huffmann, D.: Experimental and Theoretical Neutron Spectra.

/10/ EACRP/ENEA: Neutron Spectra. EACRP-L-62, Supplement 5 (1972)

/11/ Abbate, M.J., et al.: Neutron Thermalization in Light Water - Measurement and Calculation of Spectra -. NSE 60, 471 (1976)

/12/ Darrouzet, M.; Martin-Deidier, L; Girieux, R.: Actinides Capture Cross Sections Measurements in P.W.R. Spectrum - SHERWOOD irradiation -. JEF/DOC-68 (1985)

/13/ Smith, R.I.; Konzek, G.J.: Clean Critical Experiments Benchmarks for Plutonium Recycle in LWR's. EPRI NP-196 (1976)

/14/ Jenquin, U.P.; Bierman, S.R.: Benchmark Experiments to Test Plutonium and Stainless Steel Cross-Sections. NUREG/CR-0210, PNL-2273 R-C (1978)

/15/ Keinert, J.; Mattes, M.: Analysis of Benchmark Experiments for Testing the IKE Multigroup Cross-Section Libraries Based on ENDF/B-III and IV. ATKE 26, (1975), 174

/16/ Keinert, J.; Mattes, M.: JEF-1 Scattering Law Data. JEF Report 2, IKE 6-147 (September 1984)

/17/ Keinert, J.: Private Communication (1981)

/18/ Sher, R.; Fiarman, S.: Studies of Thermal Reactor Benchmark Data Intepretation: Experimental Corrections. EPRI NP-209 (1976)

/19/ Hardy, J., Jr.: Monte Carlo Analyses of TRX Slightly Enriched Uranium-H_2O Critical Experiments with ENDF/B-IV and Related Data Sets. WAPD-TM-1307 (1977)

/20/ Williams, M.L., et al.: Analysis of Thermal Reactor Benchmarks with Design Codes Based on ENDF/B-V Data. Nucl. Techn. 71, 386 (1985)

/21/ Berger, H.D., et al.: Überprüfung der Berechnungsverfahren für enge Reaktorgitter von Fortschrittlichen Druckwasserreaktoren (FDWR) an experimentellen Anordnungen. KfK 3389 (1982)

/22/ Frehaut, J.: Coherent Evaluation of nu-bar(prompt) for U-235, U-238 and Pu-239. JEF/DOC-107 (1985)

/23/ Carter, R.D.: Problems in Validating Criticality Safety Calculations. Trans. Am. Nucl. Soc. 49, 233 (1985)

/24/ Rose, P.F., et al.: Benchmark Data Testing for Thermal Reactor Applicca-tions. BNL-NCS-30368 (1981)

/25/ Craig, D.S.: Testing ENDF/B-V Data for Thermal Reactors. AECL-7690 (1982) GA-5319 (1964)

/26/ Finch, D.R.; Graves, W.E.: Quantitative Consistency Testing of Thermal Benchmark Lattice Experiments. DP-MS-77-33 (1977)

Appendix

Table A.1: 151-group structure used for the thermal library (energies in eV)

Group	lower bound	upper bound	group width	mid-point energy
1	2.97000E+00	3.05900E+00	8.90000E-02	3.01450E+00
2	2.83000E+00	2.97000E+00	1.40000E-01	2.90000E+00
3	2.71000E+00	2.83000E+00	1.20000E-01	2.77000E+00
4	2.57000E+00	2.71000E+00	1.40000E-01	2.64000E+00
5	2.45000E+00	2.57000E+00	1.20000E-01	2.51000E+00
6	2.41000E+00	2.45000E+00	4.00000E-02	2.43000E+00
7	2.38240E+00	2.41000E+00	2.76000E-02	2.39620E+00
8	2.35000E+00	2.38240E+00	3.24001E-02	2.36620E+00
9	2.32000E+00	2.35000E+00	3.00000E-02	2.33500E+00
10	2.31000E+00	2.32000E+00	9.99999E-03	2.31500E+00
11	2.25000E+00	2.31000E+00	5.99999E-02	2.28000E+00
12	2.16000E+00	2.25000E+00	8.99999E-02	2.20500E+00
13	2.15000E+00	2.16000E+00	9.99999E-03	2.15500E+00
14	2.06000E+00	2.15000E+00	9.00002E-02	2.10500E+00
15	2.05000E+00	2.06000E+00	9.99999E-03	2.05500E+00
16	2.00500E+00	2.05000E+00	4.49998E-02	2.02750E+00
17	1.96500E+00	2.00500E+00	4.00001E-02	1.98500E+00
18	1.92500E+00	1.96500E+00	4.00001E-02	1.94500E+00
19	1.88500E+00	1.92500E+00	4.00000E-02	1.90500E+00
20	1.85540E+00	1.88500E+00	2.96000E-02	1.87020E+00
21	1.82500E+00	1.85540E+00	3.03999E-02	1.84020E+00
22	1.78500E+00	1.82500E+00	4.00001E-02	1.80500E+00
23	1.75500E+00	1.78500E+00	3.00000E-02	1.77000E+00
24	1.72616E+00	1.75500E+00	2.88399E-02	1.74058E+00
25	1.68500E+00	1.72616E+00	4.11601E-02	1.70558E+00
26	1.65500E+00	1.68500E+00	3.00000E-02	1.67000E+00
27	1.62500E+00	1.65500E+00	3.00000E-02	1.64000E+00
28	1.59500E+00	1.62500E+00	3.00000E-02	1.61000E+00
29	1.55500E+00	1.59500E+00	4.00001E-02	1.57500E+00
30	1.52500E+00	1.55500E+00	3.00000E-02	1.54000E+00
31	1.49500E+00	1.52500E+00	3.00000E-02	1.51000E+00
32	1.45748E+00	1.49500E+00	3.75201E-02	1.47624E+00
33	1.42500E+00	1.45748E+00	3.24800E-02	1.44124E+00
34	1.40000E+00	1.42500E+00	2.50000E-02	1.41250E+00
35	1.37500E+00	1.40000E+00	2.50000E-02	1.38750E+00
36	1.34500E+00	1.37500E+00	3.00000E-02	1.36000E+00
37	1.30791E+00	1.34500E+00	3.70901E-02	1.32645E+00
38	1.26500E+00	1.30791E+00	4.29100E-02	1.28646E+00
39	1.23500E+00	1.26500E+00	3.00000E-02	1.25000E+00
40	1.19500E+00	1.23500E+00	4.00000E-02	1.21500E+00
41	1.16645E+00	1.19500E+00	2.85500E-02	1.18073E+00
42	1.14000E+00	1.16645E+00	2.64500E-02	1.15323E+00
43	1.12540E+00	1.14000E+00	1.46000E-02	1.13270E+00
44	1.11500E+00	1.12540E+00	1.03999E-02	1.12020E+00
45	1.09873E+00	1.11500E+00	1.62700E-02	1.10687E+00
46	1.08500E+00	1.09873E+00	1.37299E-02	1.09187E+00
47	1.07222E+00	1.08500E+00	1.27801E-02	1.07861E+00
48	1.06236E+00	1.07222E+00	9.85992E-03	1.06729E+00
49	1.05254E+00	1.06236E+00	9.82010E-03	1.05745E+00
50	1.04277E+00	1.05254E+00	9.76992E-03	1.04765E+00

Table A.1: (continued)

Group	lower bound	upper bound	group width	mid-point energy
51	1.02500E+00	1.04277E+00	1.77701E-02	1.03389E+00
52	1.01374E+00	1.02500E+00	1.12600E-02	1.01937E+00
53	9.95000E-01	1.01374E+00	1.87399E-02	1.00437E+00
54	9.85000E-01	9.95000E-01	9.99999E-03	9.90000E-01
55	9.65000E-01	9.85000E-01	2.00000E-02	9.75000E-01
56	9.50700E-01	9.65000E-01	1.43000E-02	9.57850E-01
57	9.35000E-01	9.50700E-01	1.57000E-02	9.42850E-01
58	9.15000E-01	9.35000E-01	2.00000E-02	9.25000E-01
59	8.95000E-01	9.15000E-01	2.00000E-02	9.05000E-01
60	8.76420E-01	8.95000E-01	1.85800E-02	8.85710E-01
61	8.65000E-01	8.76420E-01	1.14200E-02	8.70710E-01
62	8.45000E-01	8.65000E-01	2.00000E-02	8.55000E-01
63	8.25000E-01	8.45000E-01	2.00000E-02	8.35000E-01
64	8.05000E-01	8.25000E-01	2.00000E-02	8.15000E-01
65	7.82110E-01	8.05000E-01	2.28900E-02	7.93555E-01
66	7.65000E-01	7.82110E-01	1.71100E-02	7.73555E-01
67	7.45000E-01	7.65000E-01	2.00000E-02	7.55000E-01
68	7.25000E-01	7.45000E-01	2.00000E-02	7.35000E-01
69	7.05000E-01	7.25000E-01	2.00000E-02	7.15000E-01
70	6.85000E-01	7.05000E-01	2.00000E-02	6.95000E-01
71	6.65000E-01	6.85000E-01	2.00000E-02	6.75000E-01
72	6.45000E-01	6.65000E-01	2.00000E-02	6.55000E-01
73	6.24930E-01	6.45000E-01	2.00700E-02	6.34965E-01
74	6.05000E-01	6.24930E-01	1.99300E-02	6.14965E-01
75	5.95000E-01	6.05000E-01	9.99999E-03	6.00000E-01
76	5.85000E-01	5.95000E-01	1.00001E-02	5.90000E-01
77	5.75000E-01	5.85000E-01	9.99999E-03	5.80000E-01
78	5.60000E-01	5.75000E-01	1.50000E-02	5.67500E-01
79	5.45000E-01	5.60000E-01	1.50000E-02	5.52500E-01
80	5.35000E-01	5.45000E-01	9.99999E-03	5.40000E-01
81	5.25000E-01	5.35000E-01	1.00001E-02	5.30000E-01
82	5.15000E-01	5.25000E-01	9.99999E-03	5.20000E-01
83	5.03260E-01	5.15000E-01	1.17400E-02	5.09130E-01
84	4.90000E-01	5.03260E-01	1.32600E-02	4.96630E-01
85	4.75000E-01	4.90000E-01	1.50000E-02	4.82500E-01
86	4.55000E-01	4.75000E-01	2.00000E-02	4.65000E-01
87	4.35000E-01	4.55000E-01	2.00000E-02	4.45000E-01
88	4.17040E-01	4.35000E-01	1.79600E-02	4.26020E-01
89	4.05000E-01	4.17040E-01	1.20400E-02	4.11020E-01
90	3.90000E-01	4.05000E-01	1.50000E-02	3.97500E-01
91	3.75000E-01	3.90000E-01	1.50000E-02	3.82500E-01
92	3.65000E-01	3.75000E-01	9.99999E-03	3.70000E-01
93	3.57680E-01	3.65000E-01	7.32002E-03	3.61340E-01
94	3.45000E-01	3.57680E-01	1.26800E-02	3.51340E-01
95	3.35000E-01	3.45000E-01	9.99999E-03	3.40000E-01
96	3.20640E-01	3.35000E-01	1.43600E-02	3.27820E-01
97	3.15000E-01	3.20640E-01	5.64000E-03	3.17820E-01
98	3.01130E-01	3.15000E-01	1.38700E-02	3.08065E-01
99	2.90750E-01	3.01130E-01	1.03800E-02	2.95940E-01
100	2.78865E-01	2.90750E-01	1.18850E-02	2.84808E-01

Table A.1: (continued)

Group	lower bound	upper bound	group width	mid-point energy
101	2.70530E-01	2.78865E-01	8.33502E-03	2.74698E-01
102	2.65000E-01	2.70530E-01	5.53000E-03	2.67765E-01
103	2.51040E-01	2.65000E-01	1.39600E-02	2.58020E-01
104	2.45000E-01	2.51040E-01	6.04001E-03	2.48020E-01
105	2.35000E-01	2.45000E-01	1.00000E-02	2.40000E-01
106	2.27700E-01	2.35000E-01	7.30000E-03	2.31350E-01
107	2.20000E-01	2.27700E-01	7.70000E-03	2.23850E-01
108	2.10000E-01	2.20000E-01	1.00000E-02	2.15000E-01
109	2.05000E-01	2.10000E-01	5.00000E-03	2.07500E-01
110	1.95000E-01	2.05000E-01	1.00000E-02	2.00000E-01
111	1.84440E-01	1.95000E-01	1.05600E-02	1.89720E-01
112	1.75000E-01	1.84440E-01	9.44000E-03	1.79720E-01
113	1.65000E-01	1.75000E-01	9.99999E-03	1.70000E-01
114	1.55000E-01	1.65000E-01	1.00000E-02	1.60000E-01
115	1.45730E-01	1.55000E-01	9.27000E-03	1.50365E-01
116	1.35000E-01	1.45730E-01	1.07300E-02	1.40365E-01
117	1.25000E-01	1.35000E-01	1.00000E-02	1.30000E-01
118	1.15000E-01	1.25000E-01	1.00000E-02	1.20000E-01
119	1.11570E-01	1.15000E-01	3.43000E-03	1.13285E-01
120	1.03000E-01	1.11570E-01	8.57000E-03	1.07285E-01
121	9.50000E-02	1.03000E-01	8.00000E-03	9.90000E-02
122	8.75000E-02	9.50000E-02	7.50000E-03	9.12500E-02
123	8.19720E-02	8.75000E-02	5.52800E-03	8.47360E-02
124	7.75000E-02	8.19720E-02	4.47200E-03	7.97360E-02
125	7.25000E-02	7.75000E-02	5.00000E-03	7.50000E-02
126	6.75000E-02	7.25000E-02	5.00000E-03	7.00000E-02
127	6.25000E-02	6.75000E-02	5.00000E-03	6.50000E-02
128	5.95000E-02	6.25000E-02	3.00000E-03	6.10000E-02
129	5.69250E-02	5.95000E-02	2.57500E-03	5.82125E-02
130	5.25000E-02	5.69250E-02	4.42500E-03	5.47125E-02
131	4.75000E-02	5.25000E-02	5.00000E-03	5.00000E-02
132	4.27570E-02	4.75000E-02	4.74300E-03	4.51285E-02
133	4.05000E-02	4.27570E-02	2.25700E-03	4.16285E-02
134	3.75000E-02	4.05000E-02	3.00000E-03	3.90000E-02
135	3.45000E-02	3.75000E-02	3.00000E-03	3.60000E-02
136	3.06130E-02	3.45000E-02	3.88700E-03	3.25565E-02
137	2.80000E-02	3.06130E-02	2.61300E-03	2.93065E-02
138	2.55000E-02	2.80000E-02	2.50000E-03	2.67500E-02
139	2.25000E-02	2.55000E-02	3.00000E-03	2.40000E-02
140	2.04930E-02	2.25000E-02	2.00700E-03	2.14965E-02
141	1.75000E-02	2.04930E-02	2.99300E-03	1.89965E-02
142	1.45000E-02	1.75000E-02	3.00000E-03	1.60000E-02
143	1.23970E-02	1.45000E-02	2.10300E-03	1.34485E-02
144	1.05000E-02	1.23970E-02	1.89700E-03	1.14485E-02
145	8.00000E-03	1.05000E-02	2.50000E-03	9.25000E-03
146	6.32500E-03	8.00000E-03	1.67500E-03	7.16250E-03
147	4.05000E-03	6.32500E-03	2.27500E-03	5.18750E-03
148	2.27700E-03	4.05000E-03	1.77300E-03	3.16350E-03
149	1.05000E-03	2.27700E-03	1.22700E-03	1.66350E-03
150	2.53000E-04	1.05000E-03	7.97000E-04	6.51500E-04
151	1.00000E-05	2.53000E-04	2.43000E-04	1.31500E-04

Table A.2: 100-group structure used for the fast/epithermal library (Structure equivalent to GAM-II)

Group	Energy Interval [eV]		Lethargy Interval		Lethargy Width
1	1.34986E+07	1.49183E+07	-0.300	-0.400	0.100
2	1.22140E+07	1.34986E+07	-0.200	-0.300	0.100
3	1.10517E+07	1.22140E+07	-0.100	-0.200	0.100
4	1.00000E+07	1.10517E+07	0.000	-0.100	0.100
5	9.04837E+06	1.00000E+07	0.100	0.000	0.100
6	8.18731E+06	9.04837E+06	0.200	0.100	0.100
7	7.40818E+06	8.18731E+06	0.300	0.200	0.100
8	6.70320E+06	7.40818E+06	0.400	0.300	0.100
9	6.06531E+06	6.70320E+06	0.500	0.400	0.100
10	5.48812E+06	6.06531E+06	0.600	0.500	0.100
11	4.96585E+06	5.48812E+06	0.700	0.600	0.100
12	4.49329E+06	4.96585E+06	0.800	0.700	0.100
13	4.06570E+06	4.49329E+06	0.900	0.800	0.100
14	3.67879E+06	4.06570E+06	1.000	0.900	0.100
15	3.32871E+06	3.67879E+06	1.100	1.000	0.100
16	3.01194E+06	3.32871E+06	1.200	1.100	0.100
17	2.72532E+06	3.01194E+06	1.300	1.200	0.100
18	2.46597E+06	2.72532E+06	1.400	1.300	0.100
19	2.23130E+06	2.46597E+06	1.500	1.400	0.100
20	2.01897E+06	2.23130E+06	1.600	1.500	0.100
21	1.82684E+06	2.01897E+06	1.700	1.600	0.100
22	1.65299E+06	1.82684E+06	1.800	1.700	0.100
23	1.49569E+06	1.65299E+06	1.900	1.800	0.100
24	1.35335E+06	1.49569E+06	2.000	1.900	0.100
25	1.22456E+06	1.35335E+06	2.100	2.000	0.100
26	1.10803E+06	1.22456E+06	2.200	2.100	0.100
27	1.00259E+06	1.10803E+06	2.300	2.200	0.100
28	9.07180E+05	1.00259E+06	2.400	2.300	0.100
29	8.20850E+05	9.07180E+05	2.500	2.400	0.100
30	7.42736E+05	8.20850E+05	2.600	2.500	0.100
31	6.72055E+05	7.42736E+05	2.700	2.600	0.100
32	6.08101E+05	6.72055E+05	2.800	2.700	0.100
33	5.50232E+05	6.08101E+05	2.900	2.800	0.100
34	4.97871E+05	5.50232E+05	3.000	2.900	0.100
35	4.50492E+05	4.97871E+05	3.100	3.000	0.100
36	4.07622E+05	4.50492E+05	3.200	3.100	0.100
37	3.68832E+05	4.07622E+05	3.300	3.200	0.100
38	3.33733E+05	3.68832E+05	3.400	3.300	0.100
39	3.01974E+05	3.33733E+05	3.500	3.400	0.100
40	2.73237E+05	3.01974E+05	3.600	3.500	0.100
41	2.47235E+05	2.73237E+05	3.700	3.600	0.100
42	2.23708E+05	2.47235E+05	3.800	3.700	0.100
43	2.02419E+05	2.23708E+05	3.900	3.800	0.100
44	1.83156E+05	2.02419E+05	4.000	3.900	0.100
45	1.65727E+05	1.83156E+05	4.100	4.000	0.100
46	1.49956E+05	1.65727E+05	4.200	4.100	0.100
47	1.35686E+05	1.49956E+05	4.300	4.200	0.100
48	1.22773E+05	1.35686E+05	4.400	4.300	0.100
49	1.11090E+05	1.22773E+05	4.500	4.400	0.100
50	8.65170E+04	1.11090E+05	4.750	4.500	0.250

Table A.2: (continued)

Group	Energy Interval [eV]		Lethargy Interval		Lethargy Width
51	6.73795E+04	8.65170E+04	5.000	4.750	0.250
52	5.24752E+04	6.73795E+04	5.250	5.000	0.250
53	4.08677E+04	5.24752E+04	5.500	5.250	0.250
54	3.18278E+04	4.08677E+04	5.750	5.500	0.250
55	2.47875E+04	3.18278E+04	6.000	5.750	0.250
56	1.93045E+04	2.47875E+04	6.250	6.000	0.250
57	1.50344E+04	1.93045E+04	6.500	6.250	0.250
58	1.17088E+04	1.50344E+04	6.750	6.500	0.250
59	9.11882E+03	1.17088E+04	7.000	6.750	0.250
60	7.10174E+03	9.11882E+03	7.250	7.000	0.250
61	5.53084E+03	7.10174E+03	7.500	7.250	0.250
62	4.30742E+03	5.53084E+03	7.750	7.500	0.250
63	3.35463E+03	4.30742E+03	8.000	7.750	0.250
64	2.61259E+03	3.35463E+03	8.250	8.000	0.250
65	2.03468E+03	2.61259E+03	8.500	8.250	0.250
66	1.58461E+03	2.03468E+03	8.750	8.500	0.250
67	1.23410E+03	1.58461E+03	9.000	8.750	0.250
68	9.61117E+02	1.23410E+03	9.250	9.000	0.250
69	7.48518E+02	9.61117E+02	9.500	9.250	0.250
70	5.82947E+02	7.48518E+02	9.750	9.500	0.250
71	4.53999E+02	5.82947E+02	10.000	9.750	0.250
72	3.53575E+02	4.53999E+02	10.250	10.000	0.250
73	2.75365E+02	3.53575E+02	10.500	10.250	0.250
74	2.14454E+02	2.75365E+02	10.750	10.500	0.250
75	1.67017E+02	2.14454E+02	11.000	10.750	0.250
76	1.30073E+02	1.67017E+02	11.250	11.000	0.250
77	1.01301E+02	1.30073E+02	11.500	11.250	0.250
78	7.88932E+01	1.01301E+02	11.750	11.500	0.250
79	6.14421E+01	7.88932E+01	12.000	11.750	0.250
80	4.78512E+01	6.14421E+01	12.250	12.000	0.250
81	3.72665E+01	4.78512E+01	12.500	12.250	0.250
82	2.90232E+01	3.72665E+01	12.750	12.500	0.250
83	2.26033E+01	2.90232E+01	13.000	12.750	0.250
84	1.76035E+01	2.26033E+01	13.250	13.000	0.250
85	1.37096E+01	1.76035E+01	13.500	13.250	0.250
86	1.06770E+01	1.37096E+01	13.750	13.500	0.250
87	8.31529E+00	1.06770E+01	14.000	13.750	0.250
88	6.47595E+00	8.31529E+00	14.250	14.000	0.250
89	5.04348E+00	6.47595E+00	14.500	14.250	0.250
90	3.92786E+00	5.04348E+00	14.750	14.500	0.250
91	3.05902E+00	3.92786E+00	15.000	14.750	0.250
92	2.38237E+00	3.05902E+00	15.250	15.000	0.250
93	1.85539E+00	2.38237E+00	15.500	15.250	0.250
94	1.44498E+00	1.85539E+00	15.750	15.500	0.250
95	1.12535E+00	1.44498E+00	16.000	15.750	0.250
96	8.76425E-01	1.12535E+00	16.250	16.000	0.250
97	6.82560E-01	8.76425E-01	16.500	16.250	0.250
98	5.31578E-01	6.82560E-01	16.750	16.500	0.250
99	4.13994E-01	5.31578E-01	17.000	16.750	0.250
100	1.00000E-05	4.13994E-01	27.631	17.000	10.631